NASA Tech Briefs

National Aeronautics and
Space Administration

Electronic Components and Circuits

Electronic Systems

Physical Sciences

Materials

Computer Programs

Mechanics

Machinery

Fabrication Technology

Mathematics and Information Sciences

Life Sciences

99-11

November 1999

INTRODUCTION

Tech Briefs are short announcements of innovations originating from research and development activities of the National Aeronautics and Space Administration. They emphasize information considered likely to be transferable across industrial, regional, or disciplinary lines and are issued to encourage commercial application.

Availability of NASA Tech Briefs and TSPs

Requests for individual Tech Briefs or for Technical Support Packages (TSPs) announced herein should be addressed to

National Technology Transfer Center
Telephone No. **(800) 678-6882** or via World Wide Web at **www2.nttc.edu/leads/**

Please reference the control numbers appearing at the end of each Tech Brief. Information on NASA's Commercial Technology Team, its documents, and services is also available at the same facility or on the World Wide Web at **www.nctn.hq.nasa.gov**.

Commercial Technology Offices and Patent Counsels are located at NASA field centers to provide technology-transfer access to industrial users. Inquiries can be made by contacting NASA field centers and program offices listed below.

NASA Field Centers and Program Offices

Ames Research Center
Carolina Blake
(650) 604-0693 or
cblake@mail.arc.nasa.gov

Dryden Flight Research Center
Lee Duke
(805) 258-3802 or
lee.duke@dfrc.nasa.gov

Goddard Space Flight Center
George Alcorn
(301) 286-5810 or
galcorn@gsfc.nasa.gov

Jet Propulsion Laboratory
Merle McKenzie
(818) 354-2577 or
merle.mckenzie@comail.jpl.nasa.gov

Johnson Space Center
Hank Davis
(281) 483-0474 or
hdavis@gp101.jsc.nasa.gov

John F. Kennedy Space Center
Gale Allen
(407) 867-6626 or
galeallen-1@ksc.nasa.gov

Langley Research Center
Dr. Joseph S. Heyman
(804) 864-6006 or
j.s.heyman@larc.nasa.gov

Glenn Research Center
Larry Viterna
(216) 433-3484 or
cto@lerc.nasa.gov

George C. Marshall Space Flight Center
Sally Little
(256) 544-4266 or
sally.little@msfc.nasa.gov

John C. Stennis Space Center
Kirk Sharp
(228) 688-1929 or
ksharp@ssc.nasa.gov

NASA Program Offices
At NASA Headquarters there are seven major program offices that develop and oversee technology projects of potential interest to industry:

Carl Ray
Small Business Innovation Research Program (SBIR) & Small Business Technology Transfer Program (STTR)
(202) 358-4652 or
cray@mail.hq.nasa.gov

Dr. Robert Norwood
Office of Aeronautics and Space Transportation Technology (Code R)
(202) 358-2320 or
rnorwood@mail.hq.nasa.gov

John Mulcahy
Office of Space Flight (Code MP)
(202) 358-1401 or
jmulcahy@mail.hq.nasa.gov

Gerald Johnson
Office of Aeronautics (Code R)
(202) 358-4711 or
g_johnson@aeromail.hq.nasa.gov

Bill Smith
Office of Space Science (Code S)
(202) 358-2473 or
wsmith@sm.ms.ossa.hq.nasa.gov

Roger Crouch
Office of Microgravity Science Applications (Code U)
(202) 358-0689 or
rcrouch@hq.nasa.gov

Granville Paules
Office of Mission to Planet Earth (Code Y)
(202) 358-0706 or
gpaules@mtpe.hq.nasa.gov

NASA TechBriefs

National Aeronautics and Space Administration

November 1999
99-11

5 Electronic Components and Circuits

11 Electronic Systems

17 Physical Sciences

29 Materials

33 Mechanics

41 Machinery

49 Mathematics and Information Sciences

53 Life Sciences

Electronic Components and Circuits

Hardware, Techniques, and Processes

7 Inrush-Current-Control Circuit

7 Improved Lightning-Current Measurements on a Protective Wire

8 Watchdog Timer and Reset Control Circuit

BLANK PAGE

Inrush-Current-Control Circuit

Voltage is raised gradually from zero to full supply voltage.

NASA's Jet Propulsion Laboratory, Pasadena, California

The electronic circuit shown in the figure regulates the inrush current that arises upon initial application of voltage to capacitors. This inrush-current-control circuit is intended principally to be incorporated into an electronic instrument in which capacitors are used to filter out current spikes and noise that would otherwise be impressed on the instrument power-supply bus. In the absence of a circuit like this one, voltage would be applied to the capacitors abruptly — typically by closing a relay; the resulting high inrush current could disrupt the power-supply bus and thereby also adversely affect the operations of other instruments connected to the same bus.

Shortly after turn-on, the inrush-current-control circuit causes the voltage on the instrument bus to ramp approximately linearly up to the full power-supply potential, so that the inrush current is constrained to be an approximately square pulse of controlled amplitude. In more detail, the sequence of events is the following:

Before power is applied, all capacitors are discharged. Upon initial application of power to the input terminals, Q1 becomes turned on, and C1 starts to charge through R1. The turn-on of Q1 causes the charging of C2 to full power-supply voltage. When C1 reaches full charge, Q1 becomes turned off; this allows C2 to discharge partially. When the potential on the left side of C2 reaches the threshold voltage of Q2, the output voltage begins to ramp up toward the full power-supply value.

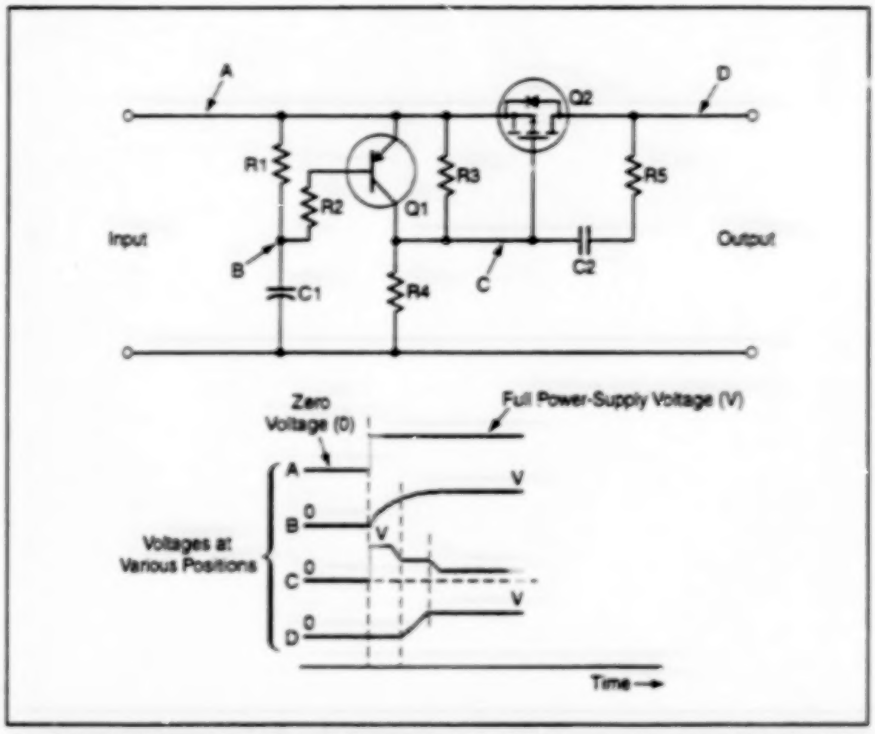

The Output Voltage of This Circuit Ramps Up to the full power-supply voltage following initial application of power.

This work was done by Steven Cole of Caltech for **NASA's Jet Propulsion Laboratory**. *Further information is contained in a TSP [see page 1].*

NPO-20403

Improved Lightning-Current Measurements on a Protective Wire

Transfer functions to correct for reflections are determined from test pulse measurements.

John F. Kennedy Space Center, Florida

A test procedure has been devised to increase the accuracy with which lightning currents on a protective wire can be determined from raw current measurements. The procedure was conceived specifically for determining lightning currents on a steel cable used to protect the space shuttle launch pad against direct lightning strikes. The cable is hung between (a) a mast on top of the launch pad and (b) two grounding points about 1,000 ft (≈300 m) away from the mast.

The measurements are made by use of current sensors at the grounded ends of the cable. The measured currents are distorted versions of the lightning currents in the following sense: Each section of the cable is, in effect, a lossy transmission line of characteristic impedance Z_0 terminated

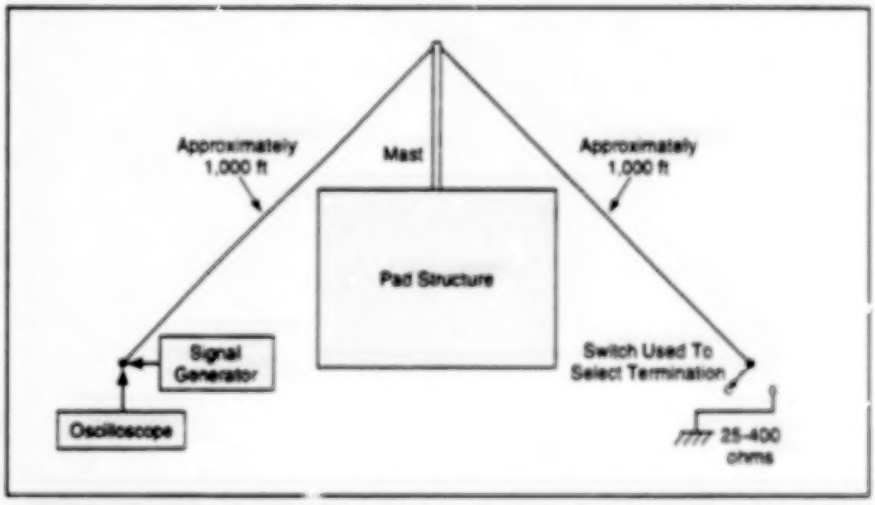

Pulses Are Applied at One End of the cable and measured after reflection from the other end of the cable with grounded and open-circuit terminations.

in impedances different from (and generally smaller than) Z_0. The mismatches between impedances give rise to reflections at the grounded ends and at the mast, so that the measured currents are superpositions of incident and reflected currents. The measurements are further complicated by attenuation (both ohmic and radiation losses) of currents that have traveled along the cable to the measurement points. In general, the characteristic impedance, the ohmic and radiation losses, and the terminating impedances are unknown and are functions of signal frequency.

The problem thus becomes one of determining frequency-dependent reflection coefficients, then using these coefficients to construct a transfer function that expresses the relationship between the raw current measurements and the incident lightning current. The transfer function can then be used, in turn, to correct the measurements for reflections and attenuations to obtain more-accurate estimates of the incident lightning current. The present test procedure (see figure) yields the needed reflection-coefficient information, without need for explicit knowledge of the unknown impedances and losses. The steps of the procedure are the following:

1. One end of the cable is disconnected from ground, creating an open-circuit (infinite-impedance) termination. The other end is connected to ground through a 50-Ω resistor.
2. A pulse with a duration of about 250 ns is applied across the resistor. About 5 μs later, this pulse returns after reflection from the open-circuit end. Because of losses, the amplitude of the returned waveform is less than that of the applied waveform. An oscilloscope at the resistor is used to observe and record the applied and returned waveforms.
3. The returned waveform is Fourier-transformed to obtain a complex spectral amplitude $S_{open}(\omega)$, where $\omega = 2\pi \times$ frequency.
4. The end opposite the resistor is connected to ground, creating a nearly short-circuit (low-impedance) termination.
5. A measurement like that of step 2 is performed. Because the impedance of the termination is less than Z_0, the polarity of the returned waveform is the reverse of that observed with the open-circuit termination.
6. The returned waveform is Fourier-transformed to obtain second complex spectral amplitude, $S_{grounded}(\omega)$.
7. The ratio $S_{grounded}(\omega)/S_{open}(\omega)$ is then calculated. This ratio is one of two desired frequency-dependent reflection coefficients.
8. The terminations and test equipment at the two ends of the cable are interchanged and steps 1 through 7 are performed to obtain the other frequency-dependent reflection coefficient; that is, $S_{grounded}(\omega)/S_{open}(\omega)$ for measurements from the opposite end.

This work was done by Pedro J. Medelius formerly of I-NET, Inc., for **Kennedy Space Center**. *Further information is contained in a TSP [see page 1].*

Inquiries concerning rights for the commercial use of this invention should be addressed to the Technology Programs and Commercialization Office, Kennedy Space Center, (407) 867-6373. Refer to KSC-11952.

Watchdog Timer and Reset Control Circuit

This circuit provides several modes of reset for a microcontroller.

Goddard Space Flight Center, Greenbelt, Maryland

A watchdog timer and reset control circuit has been designed for use with a microprocessor or microcontroller (hereafter "microcontroller" for short) that would otherwise lack the protection afforded by such a circuit. The circuit also has a register to remember the cause of a reset.

A watchdog timer is a safety feature that prevents runaway software; when it times out, it stops a microcontroller from executing meaningless code, a situation that arises from an electrical or programming error. More specifically, if the software is not being executed properly, it fails to clear the watchdog timer; if the watchdog timer is not cleared for a specified interval, the watchdog timer causes the microcontroller to reboot and execute software from a known place.

The circuit (see figure) is implemented mostly as a field-programmable gate array. In operation, the FPGA receives signals from the microcontroller and from address-decoding logic circuitry. The outputs of the FPGA are fed to the microcontroller and to a data bus. For simplicity, in the figure, all signals are represented in positive logic. Inasmuch as microcontroller input signals (e.g., the master reset input signal) are often asserted negatively, inverters can be added as needed, within or without the FPGA.

The watchdog timer consists of a ripple counter and enabling circuitry. The enabling circuitry makes it possible for software to decide when to put the watchdog timer into operation. The software can enable and disable the watchdog timer by writing to the "enable" and "disable" memory addresses. At bootup and master reset of the system that includes the microprocessor and all associated circuits, the watchdog is disabled; that is, periodic software writes to the "clear" memory address are not necessary to prevent reboot.

The interval between "clears" to keep the enabled timer from expiring is set by the clock frequency and the number of flip-flops in the ripple counter. For example, if the clock frequency is 12 MHz and 24 flip-flops are strung together in the watchdog timer, then the software must cause the microcontroller to write to the "clear" memory address at intervals of no more than $(2^{24}-1)/(12\ \text{MHz}) \approx 699$ ms, or else the watchdog timer will expire.

When the watchdog timer expires, the reset control circuitry generates a pulse that becomes the master reset pulse. The pulse generator should be designed so that the duration of the pulse satisfies the reset-pulse-duration requirements of the microcontroller and all other circuits in the system. The master reset pulse also resets and disables the watchdog timer.

Other pulse generators in the FPGA create a master reset pulse for reasons other than watchdog timer expiration: A master reset pulse can be caused by software writing to a reset address or by a push on a reset button on test equipment. In addition, when power for the system is first turned on, the subcircuit comprising the resistor, capacitor, and inverter depicted at the lower left corner of the illustration generates a pulse that becomes the master reset pulse.

The circuit includes a register that records status bits. The microcontroller can read the status bits to determine the cause of a master reset. All the status bits are cleared when software writes to a "clear status bits" address. All status bits except the power-on-reset status bit are cleared by a power-on reset.

This work was done by Kenneth W. Wagner of **Goddard Space Flight Center**. *No further documentation is available.*
GSC-13925

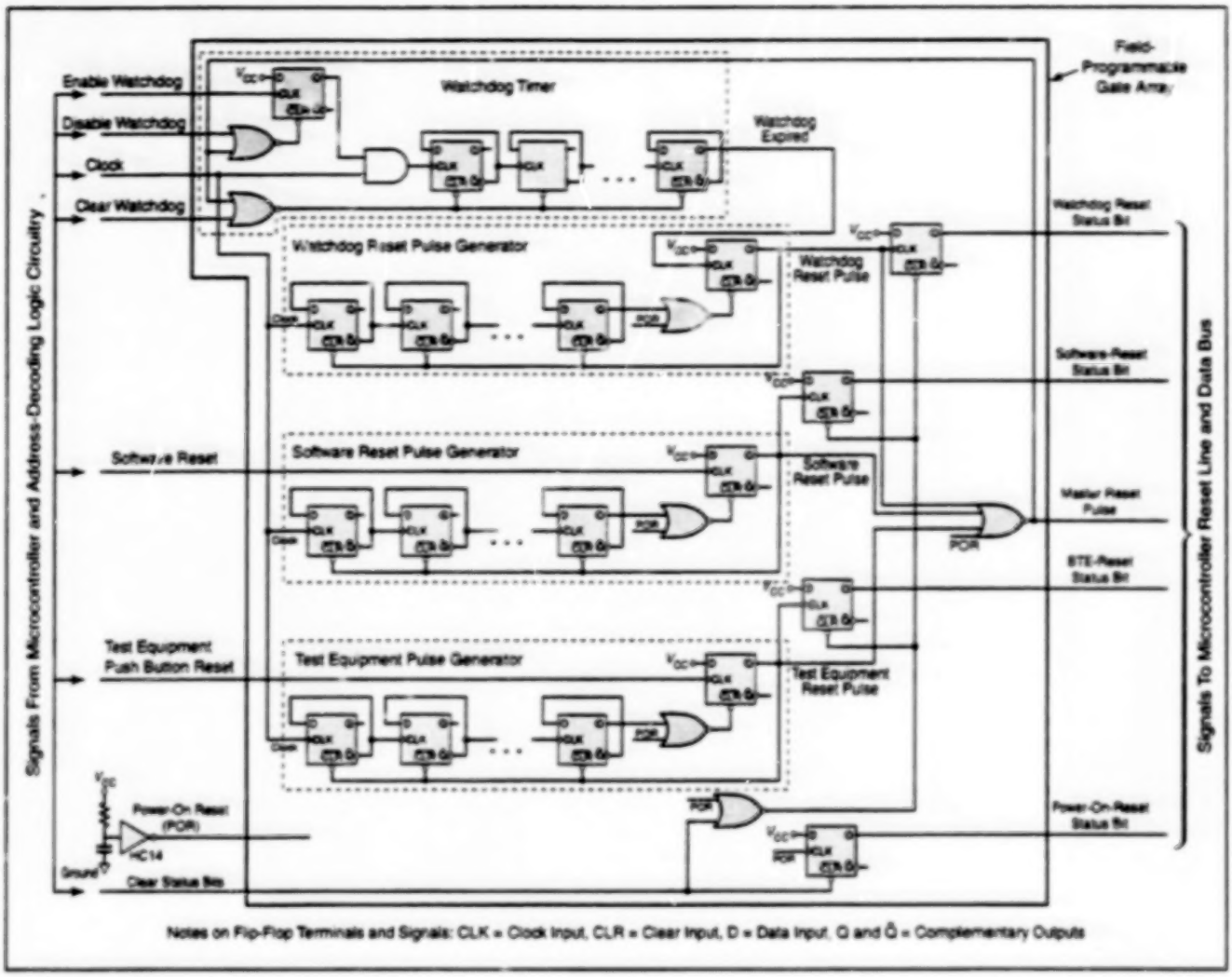

This **Watchdog Timer and Reset Control Circuit** includes a register that the microcontroller can read to determine the cause of a reset. The durations of reset pulses are precise because these pulses are generated by digital circuitry, in contradistinction to analog circuitry, which generates pulses with imprecise durations.

Electronic Systems

Hardware, Techniques, and Processes

13 Video-Based Active Alignment System

13 Programmable Motion System for Positioning Flow Probes

15 Tunable, Frequency-Stabilized Diode-Pumped Tm,Ho:YLF Laser

Video-Based Active Alignment System

Reflected images of a flashing LED are used to align two objects.

Lyndon B. Johnson Space Center, Houston, Texas

An optoelectronic system senses rotational and translational misalignment between two objects. The system might be used in such diverse applications as aligning construction equipment, mating parts of prefabricated buildings, and aligning vehicles for docking. It could replace more-expensive alignment systems like laser theodolites.

In an experimental version of the system, a video camera is mounted on the end effector of a robot, which is to be aligned with a fixture to which a reflective target is attached (see figure). A light-emitting diode (LED) is positioned at the center of the camera lens, aimed away from the camera. The target includes an ordinary mirror and several retroreflectors, which reflect light from the LED back to the camera, regardless of the orientation of the target.

Typically, the optical axis of the camera is not perpendicular to the mirror plane at the beginning of an alignment sequence. Such misalignment is sensed when the reflection of the LED in the mirror appears off center on a video monitor connected to the camera. To bring the optical axis into alignment with the perpendicular to the mirror surface, the robot is commanded to turn the camera until the video image of the LED appears at the center.

Translational misalignment in a plane parallel to the mirror surface is corrected next. Such misalignment is sensed when the video image of the retroreflectors appears displaced from the video image of the LED. The robot arm moves the camera until the centroid of the image of the retroreflectors coincides with the centroid of the image of the LED.

In processing the video-image data to compute the centroids of the LED and retroreflector images, it is necessary to eliminate data on such background features as the manipulator and the camera lens. For this purpose, a picture is taken with LED off, then quickly followed by a second picture taken with the LED on. The data processor then effectively subtracts the first picture from the second picture and performs a binary threshold operation. Only the images of the LED and the retroreflectors remain and are used to compute the centroids.

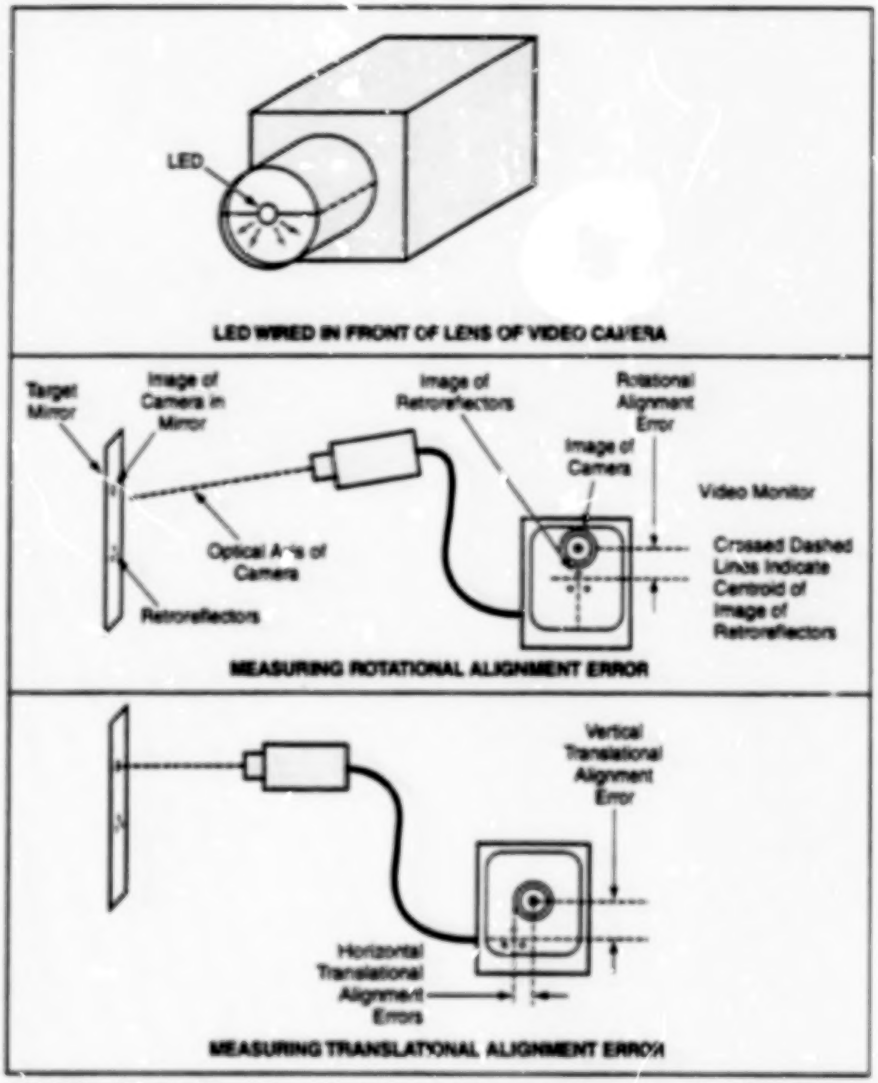

The Video Camera Observes a target that includes an ordinary mirror plus retroreflectors. Processed video images are used to adjust the orientation and position of the camera with respect to the target.

This work was done by Leo Monford of **Johnson Space Center** *and Robin Redfield, Michael Bradham, Louis Everett, and Jeffrey Pafford of Texas A&M Research Foundation. Further information is contained in a TSP [see page 1].*

MSC-21977

Programmable Motion System for Positioning Flow Probes

Advantages include flexibility, speed, expandability, and compatibility with data-acquisition and control systems.

John H. Glenn Research Center, Cleveland, Ohio

The validation of computational-fluid-dynamics (CFD) software used for the design and analysis of turbomachinery has made it necessary to resolve measurement of the flow field more finely by recording more points per survey. The demand for these measurements has resulted in additional requirements for the actuation systems used to move flow-measuring probes in testing facilities. An electronic computer-based programmable motion system (PMS) has been developed to satisfy these

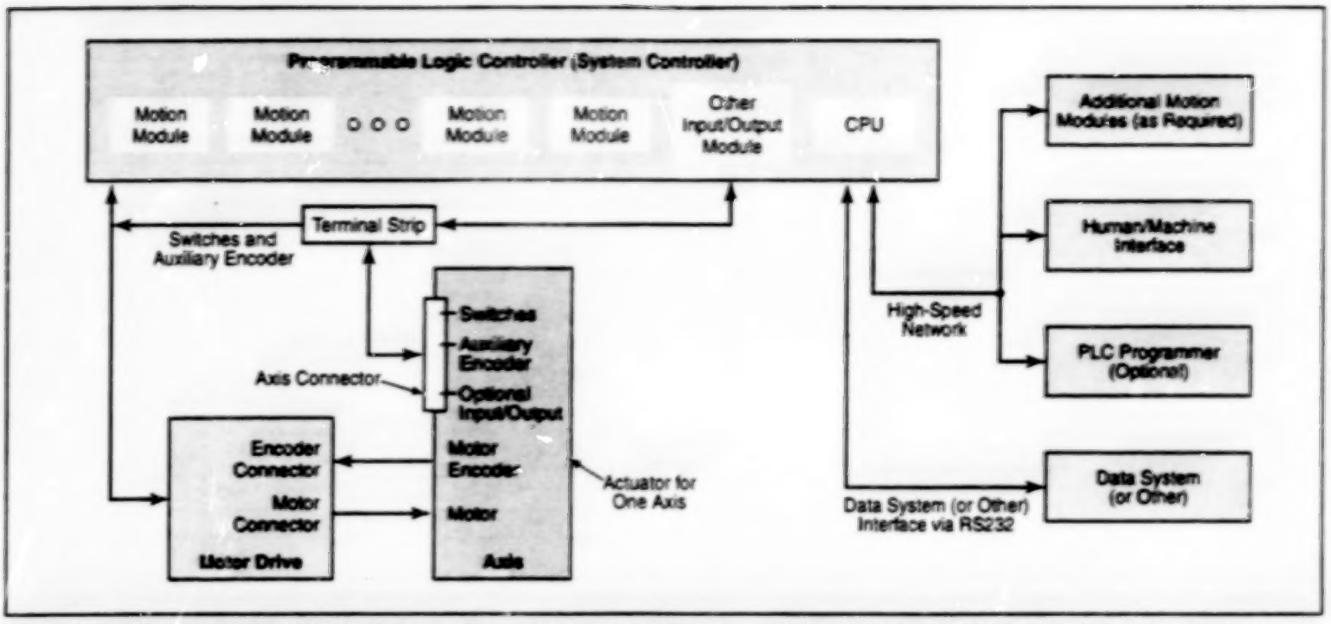

Figure 1. The **Programmable Motion System** offers enhanced capabilities for controlling as many as 18 axes of motion. For simplicity, only one actuator is shown here. A dedicated motion-control module, motor drive, and motor are needed for actuation on each axis.

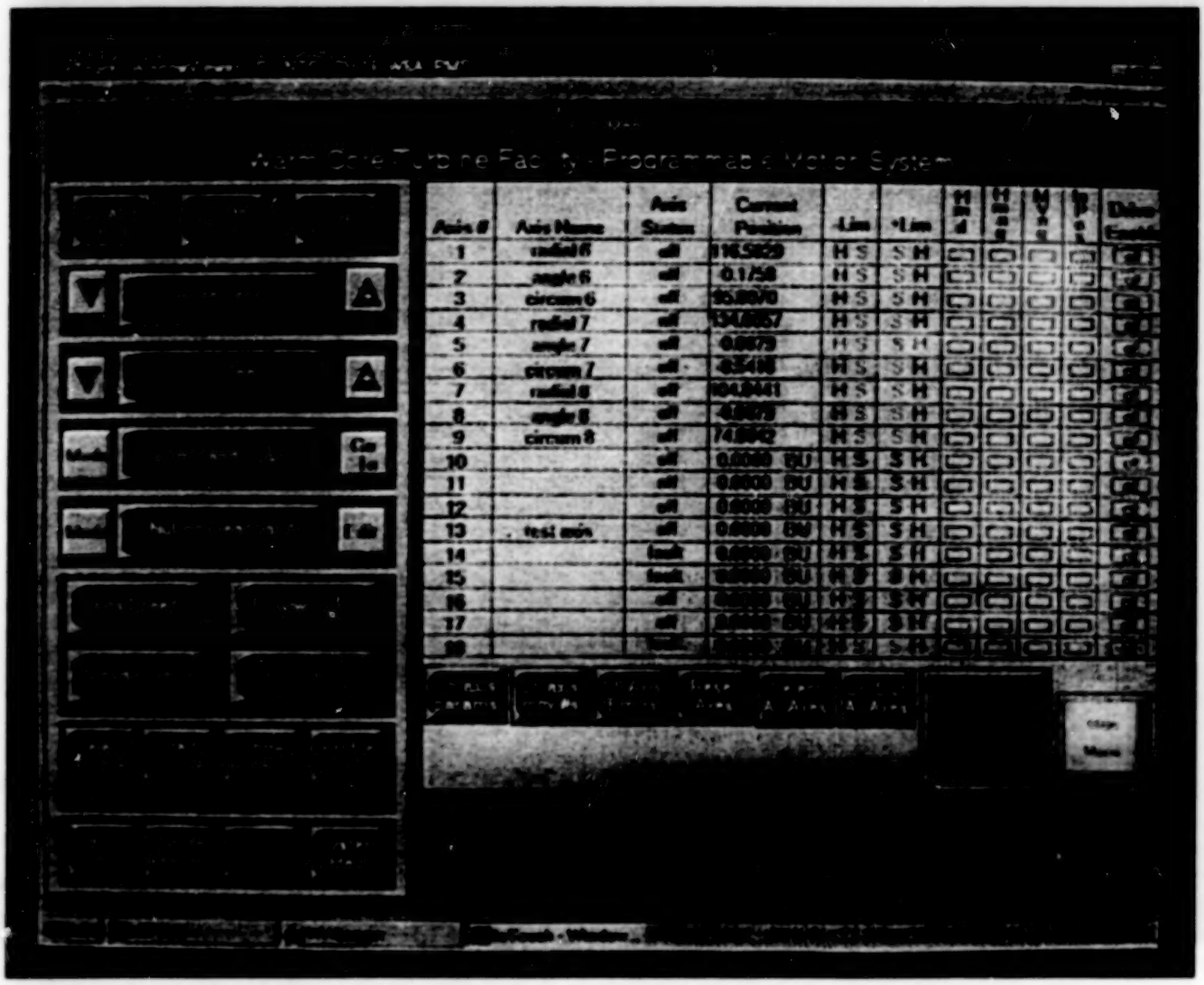

Figure 2. The **Run Menu** is a display, generated by the human/machine interface, through which the user controls motions along or about the various axes. The run menu includes an axis control panel, an access display, and an area for functions defined by the user.

requirements. The system is designed to be user-friendly and versatile, giving the user many features not available in older probe-positioning systems. Although originally developed to control probe actuators, the PMS can also be used to control the actions of movable stator vanes, laser tables, or other devices that accept velocity control signals from −10 to 10 Vdc.

The PMS can be used to control as many as 18 axes of motion. The system (see Figure 1) comprises three main parts: a programmable logic controller (PLC), a human/machine interface (HMI), and a motor-drive subsystem. The PLC is used for main control of the system. The HMI is implemented in software on a personal computer. The motor-drive subsystem includes motor-drive circuits and dc brushless motors.

The PLC, HMI, and motor-drive subsystem all operate together to effect control of speeds and positions for the various axes. The position control loop for each axis is implemented in the PLC. The velocity control loop for each axis is implemented in the motor-drive subsystem or in motion modules in the PLC, depending on the application. Commands from the user are sent to the PLC via the HMI program. The interface to the data-acquisition system is implemented in the PLC. The interface to motion profiles specified by the user resides in the HMI program.

The PMS enables its user to control the speed, position, and other parameters of motion for each axis (see Figure 2). The user can also create and edit motion profiles and cause the execution of the motions by use of the Microsoft Excel program. The system can interact with standard data-acquisition systems at Glenn Research Center and with other data and control systems.

In its initial application, the PMS is used to control three sets of circumferential, radial, and yaw probe actuators in an aeronautical test facility at Glenn Research Center. The standard modes of operation for positioning, characterized in terms of motions, are: move to a specified absolute position, move a specified positive or negative increment from the present position, find the home position, and jog (positive or negative). In addition, a yaw probe can be moved in a nulling mode, in which its position is adjusted in response to the output of a differential-pressure transducer. The versatility of the system makes it suitable for a variety of applications.

The PMS has the following advantageous features:

- For the researcher, one of the best features of the PMS may be that it functions with minimal (relative to other probe-actuation systems) communication overhead and, as a result, the measurement time is relatively short at 6 seconds per data point.
- The PMS is electrically clean; that is, its electronic circuitry does not affect such instrumentation as pressure transducers and hot-wire probes.
- Real-time editing of axis parameters, integrated profile programming, and point-and-click mouse input serve to simplify operation.
- The system can accommodate auxiliary positioning devices on the driven ends (in contradistinction to the driving ends), and in operation, the system maintains continuous communication with the data-acquisition system used in the initial application. These features are helpful for obtaining accurate and repeatable results.
- Functions specific to a test can be programmed in the field.
- The system is independent of specific motor-drive circuits or motors.
- Troubleshooting is easy.
- The system can be upgraded or expanded.

The PMS gives the user more flexibility than do older probe-actuation systems. Initial tests have shown that data-taking time is 30 to 40 percent shorter. Copies of the PMS are scheduled to be installed in at least four other aeronautical test facilities at Glenn Research Center.

This work was done by Brent C. Nowlin and L. Danielle Koch of **Glenn Research Center**. *Further information is contained in a TSP [see page 1].*
LEW-16690

Tunable, Frequency-Stabilized Diode-Pumped Tm,Ho:YLF Laser

Frequency can be swept or adjusted over a range of ±4 GHz.

NASA's Jet Propulsion Laboratory, Pasadena, California

A laser-diode-pumped thulium- and holmium-doped yttrium lithium fluoride (Tm,Ho:YLF) laser that operates at a single frequency and that can be both tuned and stabilized in frequency has been demonstrated in a laboratory setup. This demonstration is a significant achievement in a continuing effort to develop frequency-stabilized, frequency-agile lasers. Such a laser could be used, for example, as a local oscillator in a coherent lidar system, wherein its capabilities would be exploited to generate a signal with a precise nominal frequency plus or minus a time-varying Doppler compensation for the relative motion of the system and its target. There may also be uses for such lasers in laser diagnostics, and in fiber-optic communication and instrumentation systems.

The laboratory setup (see figure) includes two identical laser-diode-pumped Tm,Ho:YLF lasers, denoted the injection laser (IL) and the local oscillator (LO), respectively, in correspondence to the role that each would play in a fully developed lidar, communication, or instrumentation system. Each laser comprises a Tm,Ho:YLF crystal pumped by light at a wavelength of 794 nm from a fiber-coupled laser diode. A thermoelectric cooler is used to maintain the crystal at a temperature of −10 °C, where its optical-energy-conversion efficiency is greater than it is at room temperature.

The pumped surface of the crystal is coated for high transmittance at the pump wavelength and high reflectance at a nominal output wavelength of 2,060 nm. The surface opposite the pumped surface (the output surface of the crystal) is coated to minimize reflectance at the output wavelength. The output boundary of the laser cavity is defined by a curved output-coupling mirror that is coated for 98.5-percent reflectance at the output wavelength and is mounted facing the output surface of the crystal. Two etalons are mounted in the laser cavity, between the output crystal surface and the output-coupling mirror; these etalons are angle-tuned to enforce the desired single longitudinal laser mode and broad frequency-tuning range.

In the case of the LO, the output-coupling mirror is bonded to a piezoelectric transducer (PZT). The length of the laser optical cavity, and thus the laser frequency, can be varied by varying the voltage applied to the PZT.

In this setup, the LO can be stabilized and tuned with respect to the IL, by use of the following feedback loop: The outputs of the LO and IL are mixed in a photodiode to generate a beat note denoted intermediate frequency 1 (IF_1). The amplified IF_1 signal is mixed with a signal with a frequency between 1 and 2 GHz generated

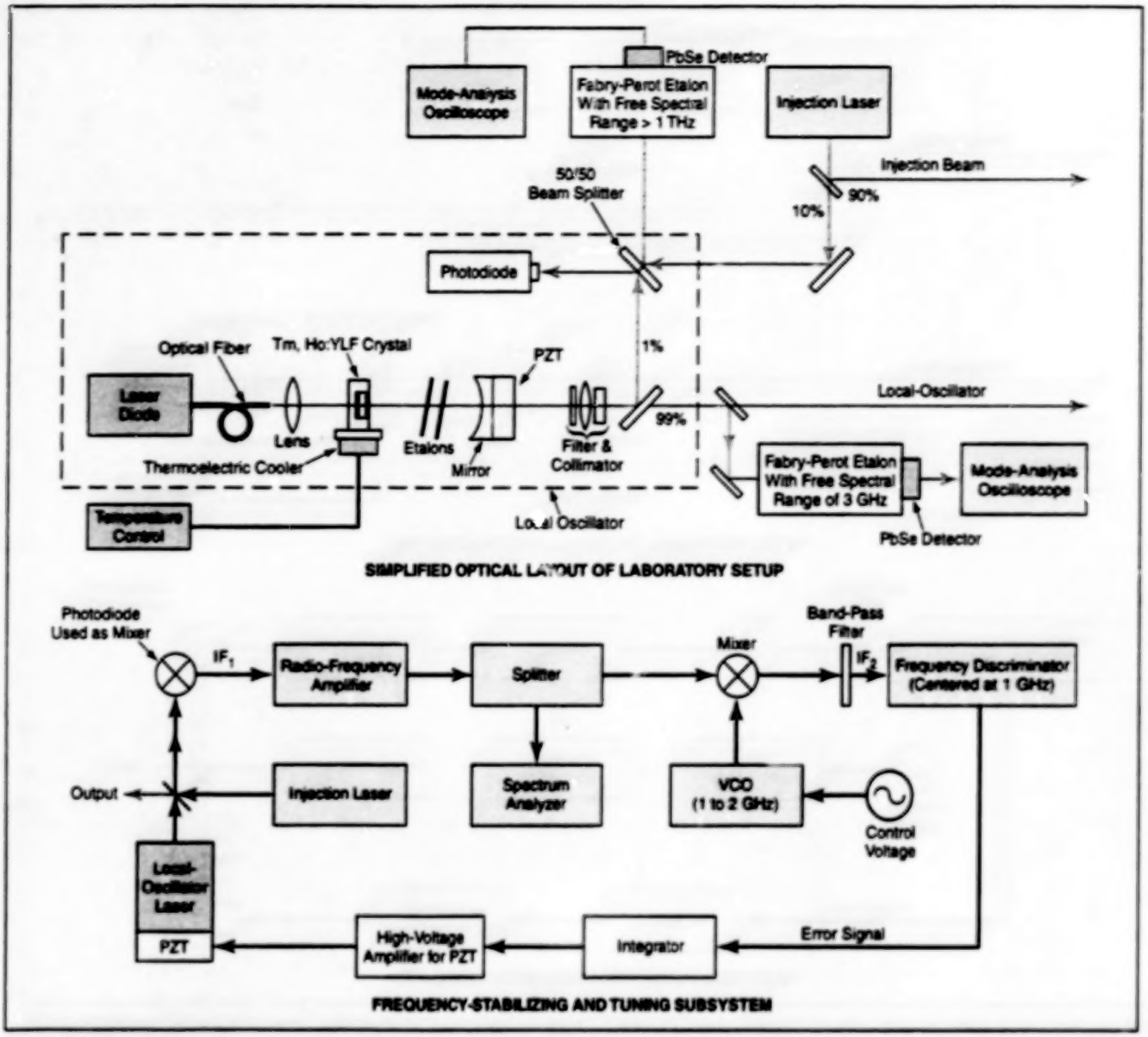

This Laboratory Setup was used to demonstrate laser-diode-pumped Tm,Ho:YLF laser that can be used as a frequency-agile local oscillator and that can be stabilized in frequency with respect to a similar laser used as an injection oscillator.

by a voltage-controlled oscillator (VCO). The resulting beat note is denoted intermediate frequency 2 (IF_2). The IF_2 signal is fed to a frequency discriminator that has a center frequency of 1 GHz. Whenever IF_2 differs from 1 GHz, the discriminator generates an error signal, which is fed to an analog integrator. The integrator output is amplified to a high voltage, which can be applied to the PZT to drive IF_2 toward 1 GHz. If the feedback loop is thus closed, then the system strives to maintain IF_1 (the difference between the LO and IL frequencies) at a frequency that differs by 1 GHz from the output frequency of the VCO.

There are three modes of operation:

- Open-Loop Operation: The feedback loop is not used. Instead, the PZT voltage is controlled at will to tune the LO frequency directly. The tuning range is ±4 GHz.
- Locked Fixed Frequency: The feedback loop is used with the VCO set at a fixed frequency. As a result, the LO is maintained at a frequency that differs from the IL frequency by a fixed amount between 0 and 1 GHz, LO jitter is reduced, and LO drift is eliminated.
- Scanning Locked Mode: The feedback loop is used and a sinusoidal or other suitable waveform with a frequency < 1 Hz is superimposed on the VCO control voltage. As in the locked-fixed-frequency mode, LO jitter is reduced and LO drift is eliminated, but in this case, IF_1 varies with the VCO control voltage. The amplitude of the waveform can be chosen to scan IF_1 over a range of ±1 GHz.

This work was done by Hamid Hemmati, Carlos Esproles, and Robert Menzies of Caltech for **NASA's Jet Propulsion Laboratory**. *Further information is contained in a TSP [see page 1].*

In accordance with Public Law 96-517, the contractor has elected to retain title to this invention. Inquiries concerning rights for its commercial use should be addressed to

Technology Reporting Office
JPL
Mail Stop 122-116
4800 Oak Grove Drive
Pasadena, CA 91109
(818) 354-2240

Refer to NPO-20444, volume and number of this NASA Tech Briefs *issue, and the page number.*

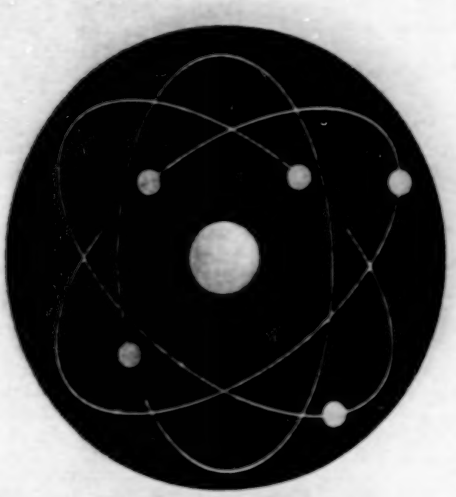

Physical Sciences

Hardware, Techniques, and Processes

19 Multiple Scattering Suppression in Laser Light Scattering
20 Miniature Scanning Electron Microscope
20 Breathing Apparatus Stores Cold Supercritical Air
21 Miniature, Rugged Infrared Spectrometer
22 Spectrometer/Radiometer for Measuring Heights of Cloud Tops
23 Computer Program for Analysis of Convective Heat Transfer
24 Loop Heat-Pipe Evaporator With Bidisperse Wick Structures
24 Ion-Mobility Spectrometric Determination of Hydrazines
25 Improved Optical Sensor for Monitoring Dissolved Oxygen
25 Continuous Electrolytic Generation of Hydrogen Peroxide
26 Software for Probabilistic Thermal and Structural Analysis
26 SINDA/FLUINT Augmented To Represent Condensable Species

Books and Reports

26 Two-Spacecraft Laser Tracking for Detecting Gravitational Waves
26 Sun Shields for the Next Generation Space Telescope
27 Telescope/Camera Systems Based on Inflation-Deployed Optics

Multiple Scattering Suppression in Laser Light Scattering

Sizes of particles in solutions can be determined over a wide range of concentrations.

John H. Glenn Research Center, Cleveland, Ohio

A laser-light-scattering method that includes cross-correlation processing of photodetector output signals has been devised for use in measuring the Brownian motions, and thereby indirectly the sizes, of particles suspended in liquids. Older laser-light-scattering methods for determining particle sizes from cross- or autocorrelation of photodetector outputs entail various deficiencies and difficulties, which include the need for precise alignment of two lasers of different wavelengths in a cross-correlation method, inability to obtain useful data at concentrations greater than 0.5 percent in one autocorrelation method, restriction to measurements at shallow depths in another autocorrelation method, and restricted angular range. The present method requires only one laser, can be used at various depths (for example in general liquid vessels or eye lenses), and yields useful data at concentrations >0.5 percent. This method can be used to determine typical particle sizes from 30 Å to 3 μm.

Singly scattered photons are needed for determining particle motions and sizes. As the concentration of particles in solution increases, the proportion of multiply-scattered photons also increases, altering photodetector outputs significantly. In autocorrelation processing, there is no way to distinguish between singly- and multiply-scattered photons arriving at the photodetector; therefore, as concentration increases, interpretation of autocorrelation signals becomes increasingly problematic. In the present method, cross-correlation is used to discriminate against photons multiply scattered from a single illuminating laser beam.

The figure depicts a simplified version of the optical configuration of this method. A laser beam is aimed through a vertically oriented cylindrical sample cell containing the particles of interest suspended in a liquid. Optionally, the cell can be placed in a vat of another liquid, the index of refraction of which approximates that of the liquid in the cell. The laser beam is focused to a waist at the middle of the cell or at any other desired depth within the cell. Two optical fibers are positioned with their receiving tips adjacent and aimed toward the beam waist (the nominal scattering volume) to receive light scattered horizontally from the beam axis to a single chosen angle. The receiving tip of one fiber is placed a short distance above the other and the two are located above or below the scattering plane.

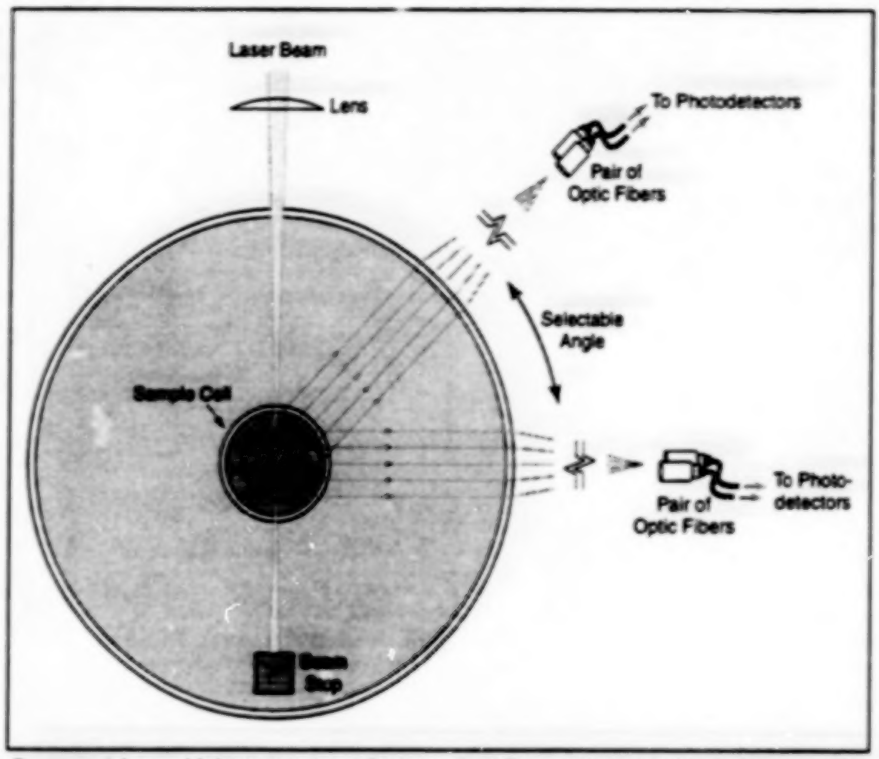

Scattered Laser Light enters two adjacent optical fibers attached to photodetectors. The separation between the receiving tips of the fibers is made smaller than single-scattering speckle but larger than multiple-scattering speckle, so that the cross-correlation (as a function of differential time) of the fluctuations in the outputs of the two photodetectors suppresses contributions by multiple scattering of photons.

Only a narrow waist beam generates the tall speckles which span both fibers. The width of the beam waist (typically ≈80 μm), the separation between the fiber tips (typically ≈250 μm), the distance of the fiber tips from the scattering volume (typically ≈170 mm, as determined by the focus of the cylindrical cell), and the laser wavelength (typically ≈0.5 μm) are chosen so that the relative sizes of time-dependent speckle arising from single and multiple scattering can be used to discriminate against signals from multiple scattering. The proper choice of dimensions is one for which (1) speckle from single scattering of photons from the same scattering volume is large enough to encompass both fiber tips while (2) speckle from multiple scattering, which results from a beam of larger diameter, is significantly smaller than the distance between fiber tips, so that (3) the single-scattering components of the outputs of photodetectors fed by the two fibers are correlated with each other, while (4) the multiple-scattering components of these outputs are not correlated with each other. Thus, cross-correlation of the two photodetector outputs is nearly equivalent to a single-photodetector autocorrelation, and can be inverted to obtain the desired particle-motion and particle-size data.

This work was done by William V. Meyer and Padetha Tin of Ohio Aerospace Institute; David S. Cannell of the University of California, Santa Barbara; James A. Lock and Thomas W. Taylor of the Cleveland State University; and Anthony E. Smart for **Glenn Research Center**. *Further information is contained in a TSP [see page 1].*

Inquiries concerning rights for the commercial use of this invention should be addressed to NASA Glenn Research Center, Commercial Technology Office, Attn: Tech Brief Patent Status, Mail Stop 7–3, 21000 Brookpark Road, Cleveland, Ohio 44135. Refer to LEW-16517.

Miniature Scanning Electron Microscope

This instrument could be used to analyze specimens in the field.

NASA's Jet Propulsion Laboratory, Pasadena, California

A miniature scanning electron microscope (SEM) with a capability for x-ray microanalysis has been proposed. This SEM would be particularly suitable for analyzing samples of dust, soil, drill tailings, and other finely divided solids collected in various environments. Designed for use in the robotic exploration of remote planets, asteroids, and comets, this instrument could also be used on Earth, where it could be operated in the field as well as in the laboratory.

The miniature SEM (see figure) would include an electron-beam column comprising a highly integrated assembly of electrostatic electron optics; as a result, this electron-beam column would be much smaller and less complex, in comparison with the electromagnetic-optics-based electron-beam column of a conventional laboratory SEM. An electrostatic deflection system in the column would be used to raster-scan the electron beam across a sample.

A coaxial microchannel plate would be used to detect secondary and back-scattered electrons. A small, highly pure, deeply depleted silicon detector, with sensitivity from <1 to >10 keV, would be used to analyze the electron-beam-induced x rays emitted by the sample, for identification of chemical elements in the sample. The field of view of the SEM would measure about 100 by 100 μm, and the spatial resolution would be about 10 nm.

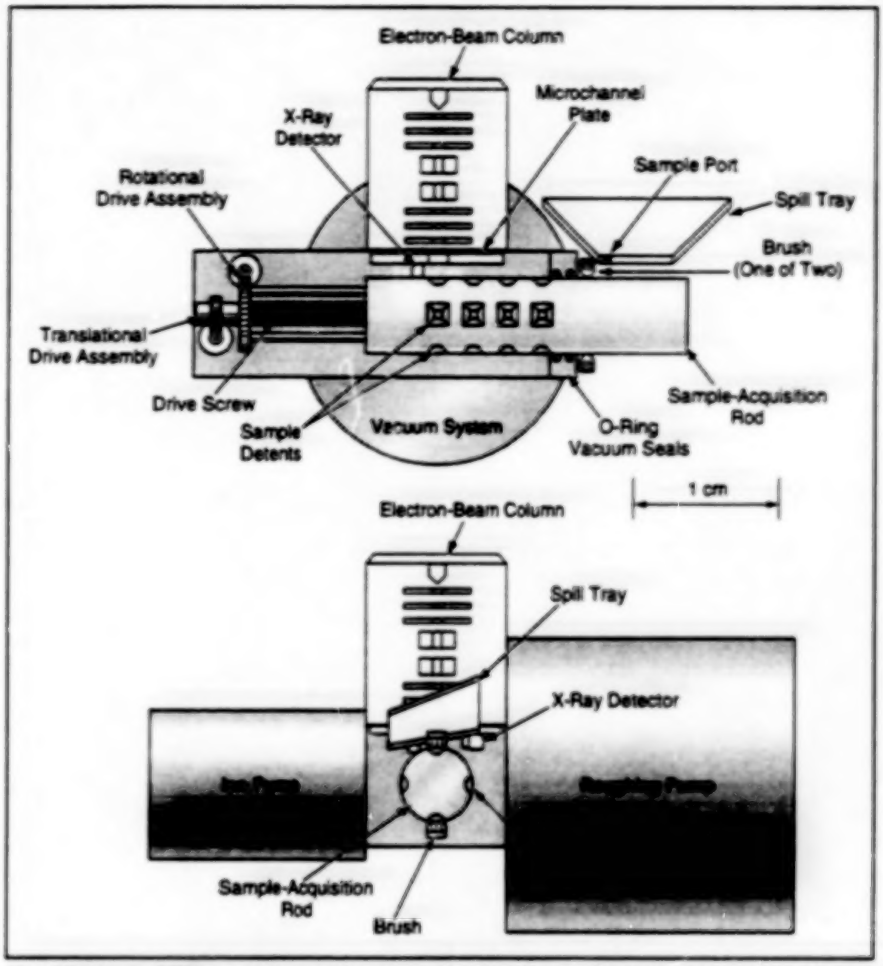

The **Miniature SEM** would have dimensions of only a few centimeters and would consume much less power than does a conventional SEM.

The vacuum needed in the interior volume of the electron-beam column and sample chamber would be provided by a dedicated vacuum system comprising a small sputter ion pump and roughing pump. Samples would be brought into the chamber by a sample-acquisition system that would include a (1) a rod equipped with O-ring vacuum seals near its outer end and with detents on its side to hold samples and (2) drive assemblies that would rotate and translate the rod. A typical sample-acquisition sequence would begin with extension of the rod to expose the detents. Sample material would be dropped into upward-facing detents, optionally with the help of a spill tray containing holes to guide the samples into the detents.

The rod would then be retracted to bring the sample-filled detents into the chamber. The rod could be further translated and rotated to bring a desired sample or part of a sample into registration with the electron-beam column. To prevent sample material from fouling the O-ring vacuum seals, small brushes would remove any sample material protruding from the detents and the rod would be made slightly narrower in the detent region than in the vacuum-sealing outer region. Once the samples had been analyzed, the rod would be extended, then rotated to dump the samples from the detents and to bring a set of empty detents to the top to receive the next set of samples.

This work was done by John L. Callas of Caltech for **NASA's Jet Propulsion Laboratory**. *Further information is contained in a TSP [see page 1].*

NPO-20499

Breathing Apparatus Stores Cold Supercritical Air

Disadvantages of liquid-air packs are overcome.

John F. Kennedy Space Center, Florida

The supercritical air mobility pack (SCAMP) is a prototype self-contained breathing apparatus designed for use in rescue and fire-fighting operations (see figure). The SCAMP is based on the storage of air at supercritical pressure in a temperature range slightly above that of liquid air. Like breathing apparatuses based on the storage of liquid air ("liquid-air packs," for short), the SCAMP offers the advantages of compactness and light weight. In addition, the SCAMP offers the following

advantages, as explained below.

In the SCAMP, air is stored essentially as a supercold compressed gas by maintaining its pressure above the critical level of 560 psia (3.86 MPa absolute). In the supercritical condition, the stored air behaves as a single-phase fluid, with no differential boiling or other separation of constituents and thus no change in chemical composition during storage. Because of the feature, the SCAMP is not susceptible to oxygen enrichment. Thus, air may be added to the vessel after storage, rather than emptying and refilling the vessel as required by current liquid-air pack technology. Moreover, there are no separate liquid and vapor volumes in the single-phase fluid; instead, the single-phase expands to occupy the entire volume of the storage vessel, making it possible to position the open end of the supply tube anywhere in the vessel to withdraw the fluid in any orientation.

The storage vessel of the SCAMP is a Dewar tank that is filled with supercritical cold air, then mounted inside a molded plastic backpack. A heat exchanger in the backpack provides for a limited flow of heat from the surroundings into the vessel to expel air for breathing. Another heat exchanger in the backpack warms the expelled air to ambient temperature to make it breathable. The heat exchangers operate in conjunction with a pressure-actuated bypass valve; together, the heat exchangers and valve maintain the stored air at a pressure of 750 psia (5.17 MPa absolute) during expulsion at ambient temperatures from −40 to 120 °F (−40 to 49 °C), at flow rates from 10 to 150 standard liters per minute.

A standard self-contained-breathing-apparatus pressure regulator and face mask are used to control and deliver the flow of breathable air to the wearer. A light-emitting-diode device on the backpack harness indicates the amount of stored air remaining in the vessel and an audible alarm is generated when less than 25 percent of the nominal full amount remains. The nearly empty vessel can be rapidly removed from the backpack and replaced with a full one.

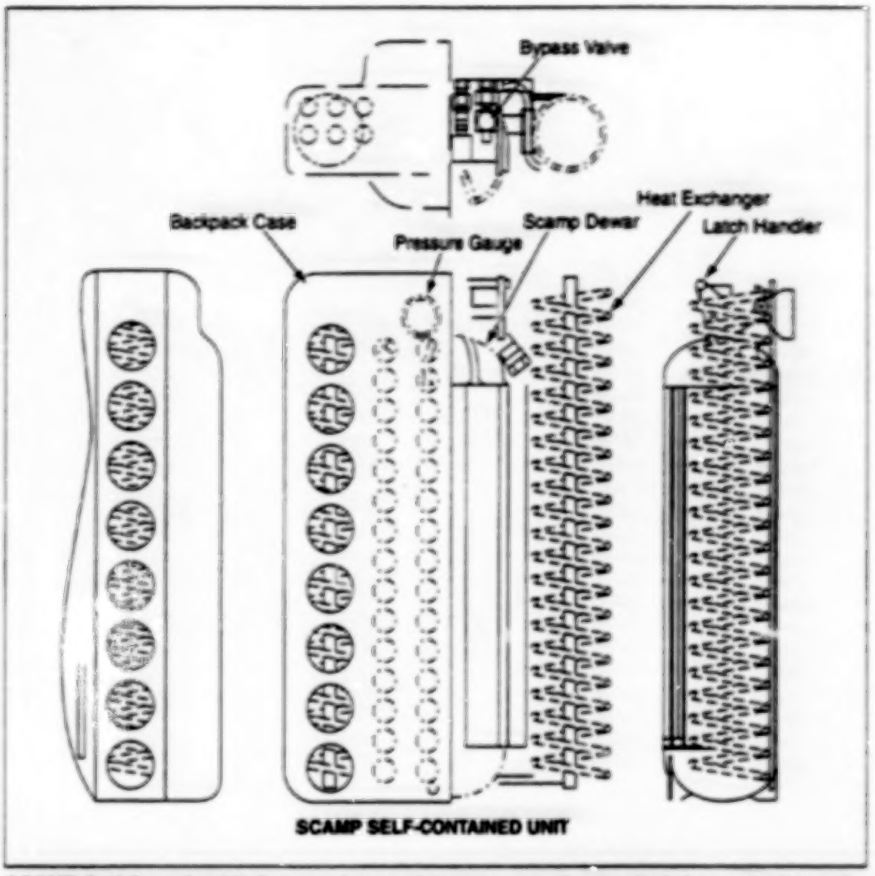

SCAMP Self-Contained Unit uses a heat exchanger to warm the expelled air to make it breathable. The apparatus is designed for rescue and fire-fighting operations.

The development of the SCAMP was accompanied by the development of an automatic loading system that reduces the difficulty of filling the storage vessel. About the size of a household refrigerator, the system requires a Dewar flask of liquid nitrogen plus electrical power of less than 100 W for operation. The system takes about 5 minutes to load a vessel rated for 1 hour.

This work was done by Harold L. Gier and Richard L. Jetley of Aerospace Design & Development, Inc., for **Kennedy Space Center**. *Further information is contained in a TSP [see page 1].*

In accordance with Public Law 96-517, the contractor has elected to retain title to this invention. Inquiries concerning rights for its commercial use should be addressed to

Harold L. Gier
Aerospace Design and Development
PO Box 672
Niwot, CO 80544-0672
Telephone No: (303) 530-2888

Refer to KSC-11683, volume and number of this NASA Tech Briefs *issue, and the page number.*

Miniature, Rugged Infrared Spectrometer

Variants could serve as engine-exhaust, chemical-process, and atmospheric chemical monitors.

John H. Glenn Research Center, Cleveland, Ohio

The figure shows a first-phase prototype of a miniature, rugged long-wavelength infrared (LWIR) spectrometer that incorporates recent advances in the design and fabrication of microelectronic and integrated optical devices. Initial development efforts have been directed toward the intended use of the instrument in measuring the concentrations of certain chemical constituents (e.g., CO_2, hydrocarbons, NO_2, N_2O, and HCl) in aircraft turbine exhaust streams. The instrument would be small and rugged enough to be mounted aboard an aircraft for diagnostic engine monitoring or even for feedback engine control. The basic instrument design could be varied to obtain automotive engine monitors, chemical-composition monitors for hot industrial processes, hand-held meters for identifying unknown chemicals or for measuring deviations from the nominal composition or purity of known chemicals, and mounted or hand-held instruments for detecting toxic or otherwise hazardous gases in outdoor or indoor air.

One especially notable component of the

This **Prototype of a Miniature, Rugged LWIR Spectrometer** was tested and found to satisfy signal-to-noise and spectral-resolution requirements to justify further development into an on-board aircraft engine exhaust-gas monitor.

instrument is a unitary silicon chip that performs all of the functions of a conventional infrared analyzer. Optical elements of the analyzer — a diffraction grating, mirrors, apertures, and beam dumps — are micromachined directly onto the chip. The main body of the chip is also an important optical element in that it has a high index of refraction and acts as a slab waveguide; the use of a high-index slab waveguide reduces (in comparison with the use of simple propagation of light through air) the needed optical path length and makes it possible to design a smaller instrument. By virtue of its unitary construction, the micromachined infrared analyzer is rugged and permanently aligned. It is insensitive to vibration and to thermal transients. It is also opaque to visible light and other interference.

Another especially notable component of the instrument is a micromachined, silicon-based linear array of 64 thermopile-type photodetectors — one for each of 64 channels that span the wavelength range from 2.8 to 5.6 μm with a resolution (bandwidth per channel) of about 0.04 μm. Each photodetector is 1.5 mm long with a pixel pitch of 75 μm. Each photodetector comprises a 0.6-μm-thick silicon nitride membrane with eleven (Bi-Te)/(Bi-Sb-Te) thermocouples.

Thermopiles typically operate over a broad temperature range (including room temperature) and are insensitive to drifts in substrate temperature, so that it is not necessary to provide for either cooling or stabilization of temperature. Thermopiles are passive devices that generate voltage outputs without need to supply bias voltage. Thus, in comparison with other infrared detectors in the same class (bolometers, pyroelectric devices, and ferroelectric devices), thermopiles consume less power and can be supported by simpler readout circuits. Moreover, if thermopiles are read out with high-input-impedance amplifiers, they exhibit negligible 1/frequency noise because there is negligible readout current. Moreover, thermopiles typically exhibit highly linear response over many orders of magnitude of incident infrared power.

It is necessary to process the thermopile readouts to extract chemical-composition information from overlapping spectral peaks. In the case of the first-phase prototype of the instrument, the outputs of the thermopiles are amplified, multiplexed, and digitized, then processed in an external laptop computer. A planned second-phase prototype would incorporate a digital signal processor that would perform neural-network processing to extract the required information.

This work was done by Edward A. Johnson and James Daly of Ion Optics, Inc., for **Glenn Research Center**. *No further documentation is available.*

Inquiries concerning rights for the commercial use of this invention should be addressed to NASA Glenn Research Center, Commercial Technology Office, Attn: Steve Fedor, Mail Stop 4–8, 21000 Brookpark Road, Cleveland, Ohio 44135. Refer to LEW-16828.

Spectrometer/Radiometer for Measuring Heights of Cloud Tops

Three instruments with a common field of view produce complementary measurements.

Goddard Space Flight Center, Greenbelt, Maryland

A spectrometer/radiometer now undergoing development is designed to be used aboard a spacecraft to measure the heights of cloud tops on Earth. The spectrometer/radiometer performs functions of three instruments — two spectrometers and a radiometer — that share a common field of view. Each of these instrument techniques implements a technique that has been used before, by itself, to measure the heights of cloud tops. By combining the three techniques in a single instrument package, the design of the spectrometer/radiometer makes it possible to determine cloud-top heights more accurately than can be done by use of one of the techniques alone. Moreover, the three techniques are complementary, so that at least one of the techniques can yield a useful measurement under conditions in which the other two techniques are deficient.

The three techniques are the following:

1. *Thermal-Infrared Technique*

The spectral radiance of a cloud top viewed from above is measured at a wavelength of 11 μm, and the temperature of the cloud top is inferred from the measured radiance. Then the height of the cloud top is inferred from the climatological temperature-versus-altitude profile of the atmosphere, under the assumption that the cloud is in thermal equilibrium with the atmosphere. This technique fails in the presence of an isothermal atmosphere or of a convective cloud, which is not in thermal equilibrium with the atmosphere.

2. *Molecular-Oxygen "A"-Band Absorption*

Back-scattered sunlight is spectrally analyzed to determine the amount of absorption of light in oxygen molecules in the wavelength range from 750 to 780 nm. The depth of the atmospheric column above a cloud (and thus the height of the cloud top) is inferred from the differential absorptions in this wavelength range. This technique is vulnerable to errors in that the accuracy of the inferred could-top height depends on accurate correction of nonoxygen absorption at the cloud boundary layer.

3. *Fraunhofer-Line Filling-in Effect (Ring Effect)*

The Fraunhofer Ca, H, and K lines (which are absorption spectral lines in the solar spectrum) in the wavelength range of 390 to 400 nm are partially filled in by scattering

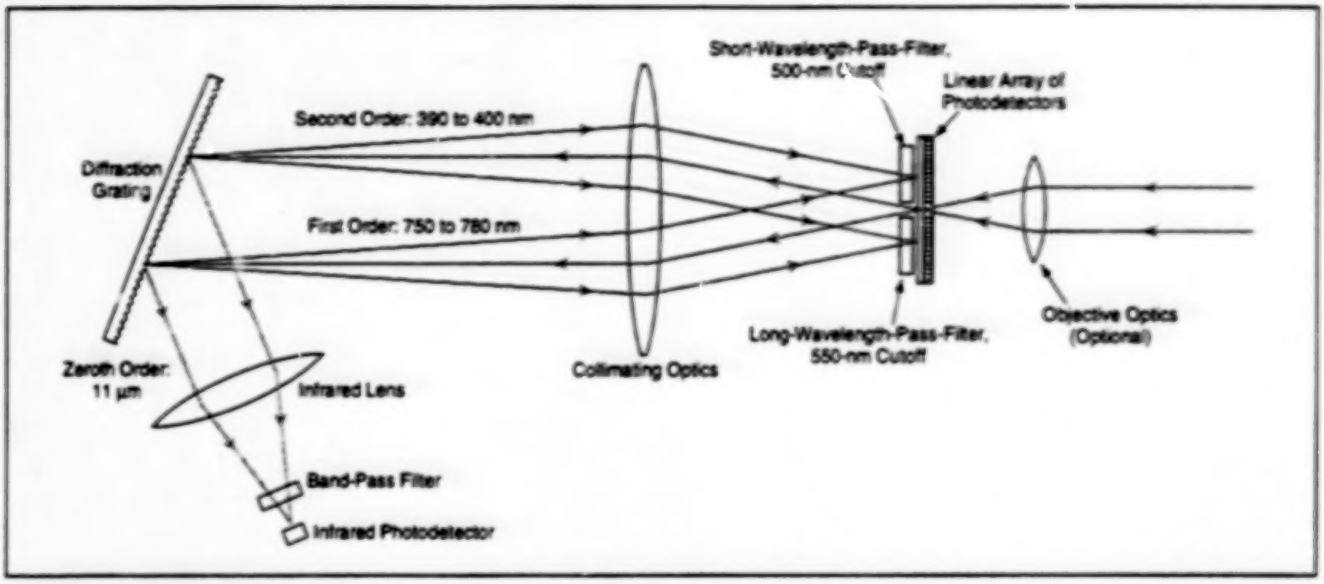

This **Spectrometer/Radiometer** diffracts light in three different orders to measure spectral properties of light scattered by cloud tops and by the atmosphere above cloud tops in three wavelength bands.

in the terrestrial atmosphere due to the frequency shift in rotational Raman scattering. The measured spectrum of back-scattered sunlight in this wavelength range is compared with the corresponding extraterrestrially measured spectrum of light coming directly from the Sun to determine the amount of filling in of the Fraunhofer lines. Then the depth of the atmospheric scattering column above the cloud top (and thus the height of the cloud top) is inferred from the amount of filling in. This technique is not vulnerable to the boundary-layer inaccuracy of the molecular-oxygen "A"-Band technique, but its accuracy depends on high spectral resolution.

In the spectrometer/radiometer (see figure), wavelength dispersion is achieved by use of a diffraction grating. The spatial period and orientation of the grating are chosen to diffract the three wavelength bands of interest in different orders that emerge in different directions. Filters provide additional spectral selectivity for sorting the orders.

The 11-μm radiation is diffracted in the zeroth order of the grating, goes through a band-pass filter, and impinges on an HgCdTe photodetector cooled by liquid nitrogen. The 750-to-780-nm radiation is diffracted in the first order of the grating, goes through a long-wavelength-pass filter with a cutoff wavelength of about 550 nm, and impinges on part of a 1,024-pixel linear array of silicon photodiodes on a focal plane. The 390-to-400-nm radiation is diffracted in the second order, goes through a short-wavelength-pass filter with a cutoff wavelength of about 500 nm, and impinges on another part of the linear array of photodiodes. The spectral resolution is 0.4 nm in the first order and 0.2 nm in the second order.

This work was done by Hongwoo Park of **Goddard Space Flight Center**, *Peter F. Soulen of the University of Maryland, and Coorg R. Prasad of Science & Engineering Services, Inc. Further information is contained in a TSP [see page 1].*

GSC-14022

Computer Program for Analysis of Convective Heat Transfer

Convective heat transfer is calculated without wall functions.

John H. Glenn Research Center, Cleveland, Ohio

Glenn-HT is a computational fluid dynamics (CFD) computer code for the analysis of three-dimensional flow and convective heat transfer in a gas turbine. Glenn-HT has been evolving during the past few years at Glenn Research Center, and at least 35 technical papers relative to this code have been published. The code is unique in the ability to give highly detailed representations of flow fields very close to solid surfaces. This ability is necessary for obtaining accurate representations of fluid heat transfer and viscous shear stresses.

The computation of convective heat transfer in a gas-turbine environment is a very difficult task, but one that must be done with reasonable accuracy in order to design a durable engine. Three-dimensional CFD computer codes are used extensively to determine pressure distributions in turbines, but the determination of heat transfer is a much more complex problem, in which it is necessary to consider details of flow fields very close to solid walls. Glenn-HT has been specifically developed to address this issue. The unique feature of this code is the use of a multiblock grid system that enables the use of high-quality grid structures very close to walls, eliminating the need for wall functions for calculating heat transfer. A conventional aspect of the code is the inclusion of a two-equation k–ω model (a k–ω model is a mathematical model of turbulence in which k denotes the turbulent kinetic energy, while ω denotes the fractional rate of dissipation of the k).

The code has been used extensively to perform cooling-passage-flow and hot-gas path flow calculations, including detailed calculations of film cooling and of complex tip-clearance-gap flow and heat transfer. The code has been validated for a number of turbine configurations. Although developed and used primarily as a research tool, the code should be useful for detailed design analysis.

This work was done by James D. Heidmann of **Glenn Research Center**, *Ali A. Ameri and Vijay K. Garg of AYT Corp., David L. Rigby of NYMA/Dynacs, and Erlendur Steinhorsson of CAI.*

LEW-16765

Loop Heat-Pipe Evaporator With Bidisperse Wick Structures

Bidisperse structures help prevent vapor blanketing of wicks.

Goddard Space Flight Center, Greenbelt, Maryland

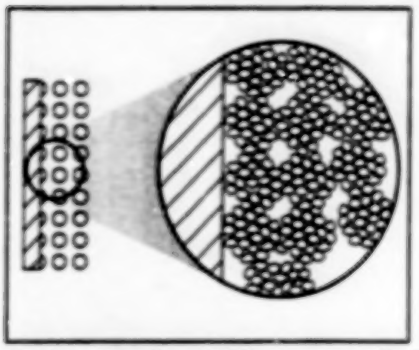

Figure 1. Bidisperse Wicks exhibit two distinct pore sizes.

Improved evaporators for loop heat pipes have been developed by incorporating bidisperse structures (in place of older monodisperse structures) into evaporator wicks. As explained in more detail below, the bidisperse structures feature two distinct pore sizes (see Figure 1), which helps to prevent vapor blanketing that can limit heat-flux capacities to unacceptably low values.

Loop heat pipes are important parts of systems for cooling electronic components that dissipate heat at flux densities up to 100 W/cm^2. Loop-heat-pipe evaporators of older design do not work at heat-flux densities in excess of 12 W/cm^2 because vapor blanketing of the wicks in those evaporators blocks the flow of heat-transfer liquids into the evaporators.

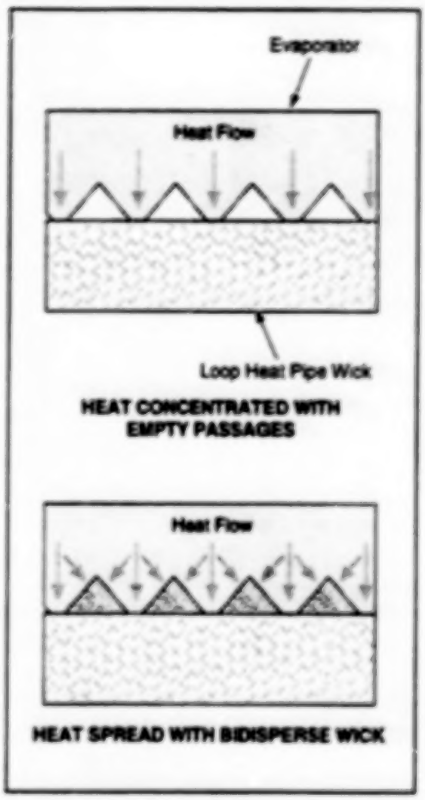

Figure 2. In the New Design, the circumferential grooves of the evaporator body are filled with sintered bidisperse wick. Effectively, this creates an efficient extended surface evaporator because bidisperse wick and the triangular groove lands both function as fins.

These wicks have monodisperse micron-size features.

The present improved evaporators are designed (see Figure 2) to prevent vapor blanketing of the wicks. The wicks in these evaporators include bidisperse structures at the interfaces between the heated evaporator walls and core wicks. The bidisperse structures contain both micron-size pores for the liquid supply and larger pores for venting of vapor. The bidisperse structures are in contact with the core wicks, which contain monodisperse micron-size pores. In a given evaporator, the bidisperse structures can be sintered in circumferential grooves in the evaporator wall and/or sintered in circumferential grooves on the outer surface of the core wick.

Because vapor can leave the wicks through the larger pores, vapor blanketing of the wicks does not occur, even at evaporator-wall heat-flux densities greater than 12 W/cm^2. Tests of loop heat pipes equipped with the bidisperse wick structures demonstrated good performance at evaporator-wall heat-flux densities up to 100 W/cm^2.

This work was done by John H. Rosenfeld, David B. Sarraf, Dmitry K. Khrustalev, Peter J. Wellen, and Mark T. North of Thermacore, Inc., for **Goddard Space Flight Center.**

GSC-14225

Ion-Mobility Spectrometric Determination of Hydrazines

The use of 5-nonanone as the ion former reduces sensitivity to ammonia.

Lyndon B. Johnson Space Center, Houston, Texas

Hydrazine, monomethylhydrazine, and unsymmetrical dimethylhydrazine can be detected and measured at concentrations as low as 10 parts per billion in the presence of ammonia at concentrations as high as 10 parts per million (greater than the odor threshold concentration of ammonia, approximately 5 ppm) by modified use of a portable, commercially available ion-mobility spectrometer. The modification consists in the substitution of 5-nonanone for acetone as the ion-forming compound in the drift or source region of the ion-mobility spectrometer. Previously, when acetone was used and ammonia was present in the sampled atmosphere even at ppm levels, chemical reactions between the ammonia and the acetone formed ion adducts that had mobilities comparable to those of monomethylhydrazine and that, consequently, interfered with the detection of hydrazines.

The simplicity and sensitivity of the modified ion-mobility spectrometric assay make it very attractive for use in monitoring atmospheres in vehicles and buildings where hydrazines, which can have serious adverse effects on health even at low concentrations, are being used. The modified assay also can be used to detect ammonia at concentrations ≥ 5 ppm.

Experience has shown that the commercially available ion-mobility spectrometer remains at top performance for 2 to 3 months, and modifications of its design may extend the performance lifetime to 12 months or more. Safety is not a factor as long as the integrity of the analyzer is maintained, and the nonanone vapor is not considered toxic at the low levels that one might expect to be vented to the atmosphere from the ion-mobility spectrometer.

Heretofore, the source of vapor has been clay adsorbent coated with nonanone, but other sources might also be used. The required concentrations of vapor are in excess of 100 parts per billion; exact values are expected to be established experimentally.

This work was done by Gary A. Eiceman of New Mexico State University, Thomas F. Limero of KRUG Life Sciences, Inc., and John L. Brokenshire of Graseby Ionics, Ltd., for **Johnson Space Center.**

Further information is contained in a TSP [see page 1].

MSC-21966

Improved Optical Sensor for Monitoring Dissolved Oxygen

Oxygen induces a reduction in the fluorescence lifetime of indicator molecules immobilized in an oxygen-permeable polymer.

John F. Kennedy Space Center, Florida

An optical sensor for measuring the partial pressure of dissolved oxygen in water is based on the effect of oxygen quenching on the fluorescence lifetime of an optically excited ruthenium complex immobilized in a recently developed polymer. In the operation of this sensor, the fluorescence lifetime and thus the degree of quenching and partial pressure of oxygen are measured by a phase-sensitive detection method described below. This sensor is a prototype of improved oxygen-concentration transducers, which are needed for monitoring critical oxygen concentrations in bioreactors and chemical plants.

The predecessors of this sensor include electrical (galvanic and polarographic) sensors and similar fluorescence-quenching sensors. The electrical sensors are subject to spurious responses due to ambient electrical noise, calibration drift arising from electrolyte depletion and/or fouling followed by reductive oxygen consumption, and poor sensitivity at low oxygen partial pressures. Among the older fluorescence-quenching sensors are versions in which the immobilizing polymers are made of silicone rubber and in the operation of which oxygen levels are deduced from measurements of fluorescent intensity. These older fluorescence-quenching sensors are subject to long-term calibration drift resulting from indicator photobleaching, and frequently require complicated multipoint calibrations because of their nonlinear Stern-Volmer response.

The deviation from linearity with the older optical sensors is partly attributable to electrostatic binding of the indicator molecules — particularly cationic ruthenium complexes — to anionic silanol groups on the surface of silica particles that are added to the silicone polymers to increase tear resistance. This binding reduces the degree of quenching by oxygen for a portion of the polymer-immobilized fluorophores, resulting in a negative deviation from a linear response. Tests of the solubility of the ruthenium complex in traditional silicones lacking silica particles showed the indicator material to be insoluble and, therefore, poorly suited for the construction of oxygen sensors.

The recently developed polymer used in the present sensor is a highly oxygen permeable fluoropolymer possessing slightly polar aromatic chain segments. These polar groups were found to solubilize the indicator complex in the polymer without affecting the degree of accessibility by oxygen. The hydrophobic nature of the fluoropolymer imparts a degree of selectivity in the sensor response by excluding nongaseous water-borne quenchers from the sensing membrane. The polymer is also inherently tear resistant by virtue of microscopic crystalline domains formed from aromatic polymer chain segments.

Unlike the response of older sensors made with silicone rubber, sensors made with the new membrane polymer exhibit a linear Stern-Volmer response that has been attributed to the greater homogeneity of the oxygen-quenching environment created around the ruthenium complex within the sensing membrane. This linear Stern-Volmer response to oxygen should make it possible to use a one- or two-point calibration procedure.

In operation, oxygen from solution diffuses freely into the polymer, where it efficiently quenches the photoexcited ruthenium complex, reducing the lifetime of the fluorescence process. Excitation light energy is provided by a light-emitting diode operating in sinusoidally driven amplitude-modulation mode at a fixed angular frequency, ω. The resulting fluorescent signal is amplitude-modulated at the same frequency, but phase shifted relative to that of the excitation. The average fluorescence lifetime, τ, of the indicator complex is calculated from the observed phase shift, θ, occurring to the expression $\tau = \tan(\theta)/\omega$. Fluorescence lifetimes for the polymer-immobilized indicator were shown to be inversely proportional to the solution partial pressure of oxygen over the range 0 to 400 mm Hg.

This work was done by James A. Kane of Polestar Technologies, Inc., for **Kennedy Space Center**.

In accordance with Public Law 96-517, the contractor has elected to retain title to this invention. Inquiries concerning rights for its commercial use should be addressed to

James A. Kane
Polestar Technologies, Inc.
220 Reservoir Road
Suite 28B
Needham Heights, MA 02194
Tel No.: (781) 449-2284
E-mail: polestar@ix.netcom.com

Refer to KSC-11998, volume and number of this NASA Tech Briefs *issue, and the page number.*

Continuous Electrolytic Generation of Hydrogen Peroxide

Faradaic efficiencies of nearly 100 percent can be achieved.

Lyndon B. Johnson Space Center, Houston, Texas

Electrolytic cells for the continuous generation of hydrogen peroxide in streams of water have been developed. Cells of this type could be incorporated into wastewater-treatment systems based on advanced oxidation processes that utilize hydroxyl radicals. In addition to H_2O_2-generating cells, such a treatment system would include catalysts for the decomposition of H_2O_2 and the formation of hydroxyl radicals as decomposition products. The hydroxyl radicals would oxidize organic contaminants, thereby removing them from the wastewater.

An electrolytic cell of this type includes an anode and a cathode in direct contact with a polymeric electrolyte membrane. Oxygen is supplied and dissolved in the wastewater stream, which is then circulated over the cathode. Under suitable conditions of oxygen pressure, flow rate, and electric-current density, H_2O_2 accumulates over the cathode with nearly 100-percent faradaic efficiency. Multiple cells could be stacked to multiply the rate of production of H_2O_2.

This work was done by James H. White, Michael Schwartz, and Anthony F. Sammells of Eltron Research, Inc., for **Johnson Space Center**.

In accordance with Public Law 96-517, the contractor has elected to retain title to this invention. Inquiries concerning rights for its commercial use should be addressed to

Eileen Sammells
Eltron Research Inc.
5660 Airport Boulevard
Boulder, CO 80301-2340
Tel. No.: (303) 440-8008

Refer to MSC-22835, volume and number of this NASA Tech Briefs *issue, and the page number.*

Software for Probabilistic Thermal and Structural Analysis

This program is expected to help improve designs of major turbine-engine components.

John H. Glenn Research Center, Cleveland, Ohio

NESTEM is a computer code that is a combination of a heat-transfer-analysis subprogram and a NASA in-house probabilistic-analysis code called "NESSUS" (for Numerical Evaluation of Stochastic Structures Under Stress). NESTEM can be used to analyze a complex combustor thermal environment with uncertainties and to assess the effects of the environment and the uncertainties on the overall responses of components. NESTEM is expected to help in the development of a comprehensive probabilistic methodology for reliable and robust design of such major turbine-engine components as compressors, turbines, impellers, and combustors.

Prior to the development of NESTEM, there was no known program that afforded a capability for perturbing such heat-transfer variables as thermal conductivities of materials, convection coefficients, and radiation temperatures. NESTEM enables one to perform a formal assessment of uncertainties in loads, variations in properties of materials, and geometric imperfections on the overall structural behavior (as characterized by stability parameters, frequencies, stresses, and other parameters).

In addition to enabling probabilistic heat-transfer analysis, NESTEM makes it possible to generate mathematical models of components by use of selected modules from the NASA in-house Composite Blade Structural Analyzer (COBSTRAN) computer code. Furthermore, the material-property parameters needed to represent ceramic-matrix composites are obtained by use of the NASA in-house Ceramic Matrix Composite Analyzer (CEMCAN) code.

This work was done by B. M. Patel of Modern Technologies Corp. for **Glenn Research Center**.

LEW-16788

SINDA/FLUINT Augmented To Represent Condensable Species

The Systems Improved Numerical Differencing Analyzer/Fluid Integrator (SINDA/FLUINT) software system has been upgraded by addition of a capability for simulating fluid mixtures that include condensable vapors. SINDA/FLUINT is the NASA standard software system for computational simulation of interacting thermal and fluid effects in arbitrary heat-transfer and fluid-flow networks. Prior to this upgrade, SINDA/FLUINT could represent single-phase vapors, single-phase liquids, and two-phase fluids, but not condensable vapors within mixtures. Now SINDA/FLUINT can also represent a fluid mixture that includes a condensable vapor, one or more noncondensable gas(es), and one or more nonvolatile liquid(s). Inasmuch as condensable vapors are often important constituents of two-phase fluids, the upgraded SINDA/FLUINT is more useful as an engineering software tool in general and for designing and analyzing liquid propulsion and environmental-control systems in particular. In addition, because of the added capability, fewer design iterations should be needed when using SINDA/FLUINT.

This work was done by Brent A. Cullimore of Cullimore and Ring Technologies, Inc., for **Johnson Space Center**. *Further information is contained in a TSP [see page 1].*

MSC-22816

Books and Reports

Two-Spacecraft Laser Tracking for Detecting Gravitational Waves

A paper proposes a method of mutual coherent laser tracking of two spacecraft for detecting gravitational radiation. Each spacecraft would transmit a laser beam to, and receive a similar laser beam from, the other spacecraft. Each spacecraft would also coherently transpond a laser beam back to the other spacecraft. Comparison of the phases of the various transmitted and received signals would yield four sets of tracking data — two sets of one-way and two sets of two-way Doppler shifts that could be partly attributable to gravitational waves. The data would be time-tagged and telemetered back to Earth for analysis. Because laser-frequency fluctuations would be the main source of noise, the analysis would exploit a theoretical development that provides for linearly combining the four sets of data in such a way as to reduce, by several orders of magnitude, the noise levels of Fourier components at frequencies that are integer multiples of the reciprocal of the round-trip light-travel time. Thus, at these frequencies, gravitational signals could more readily be identified in the presence of noise.

This work was done by Massimo Tinto of Caltech for **NASA's Jet Propulsion Laboratory**. *To obtain a copy of the report, "Spacecraft to spacecraft coherent laser tracking as a xylophone interferometer detector of gravitational radiation," see TSP's [page 1].*

NPO-20501

Sun Shields for the Next Generation Space Telescope

A report discusses the design of inflatable Sun shields proposed for use in keeping the primary mirror of the Next generation Space Telescope (NGST) at a temperature ≤60 K. The report summarizes a paper presented at the 33rd Intersociety Energy Conversion Engineering Conference in August 1998 at Colorado Springs, Colorado. The proposed shields would include six parallel layers of thin aluminized polyimide film separated by gaps wide enough to ensure against contact. The layers would be radiatively isolated from each other. The proposed shields would weigh 247 kg less than those of an older proposed design involving multilayer insulation with 10 inner layers, or 388 kg less than those of another older proposed design involving multilayer insulation with 18 inner layers. Relative to the shields of both older designs, the proposed shields would also offer advantages of simplification of packaging, simplification of mechanical structure, and less dependence of telescope temperature on a poorly adherent thermal coating on the Sun side of the outer shield layer.

This work was done by Michael K. Choi of **Goddard Space Flight Center**. *To obtain a*

copy of the report, "A Practical Thermal Design Concept for Next Generation Space Telescope Sunshield," see TSP's [page 1].
GSC-14254

Telescope/Camera Systems Based on Inflation-Deployed Optics

A report proposes the development of spaceborne telescope/camera systems that would be lightweight, relatively inexpensive alternatives to current systems based on glass mirrors. For example, one such system might offer the same performance as that of the Hubble Space Telescope, at about a tenth of the weight and a hundredth of the cost. In a system of the proposed type, the primary reflector (typically a paraboloid several meters in diameter) would be of the membrane-mirror type. The primary reflector would be part of a folded, closed, flexible structure that would be deployed by inflation, then depressurized after being rigidified in the deployed condition. Because the primary reflector would only approximate the required precise reflector surface and because deviations from the required surface would vary with thermal, solar-wind, and microgravitational conditions, the system would also include a two-stage active optical subsystem that would correct wavefront errors in real time. According to the proposal, development efforts should focus on four major topics: (1) the membrane mirror, (2) packaging and deployment of the membrane mirror, (3) the two-stage optics, and (4) systems engineering.

This work was done by James Breckinridge, Marjorie Meinel, Aden Meinel, and James Bilbro of Caltech for **NASA's Jet Propulsion Laboratory**. *To obtain a copy of the report, "Inflation-Deployed camera," see TSP's [page 1].*
NPO-20405

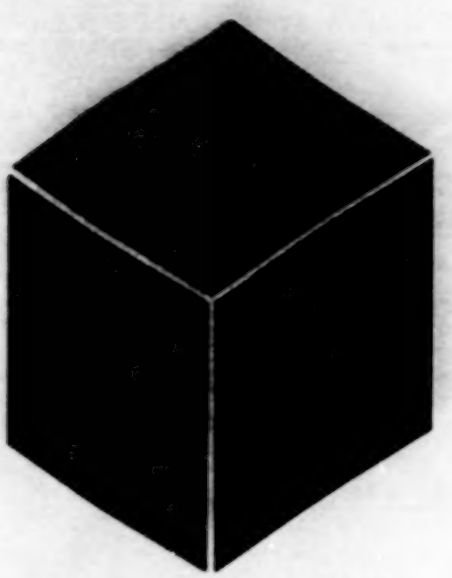

Materials

Hardware, Techniques, and Processes

31 Ceramic $Si_wB_xC_yO_z$ Fibers From Organic Si/B Polymer Precursors
31 Tailoring Fiber/Matrix Interfaces Through Kirkendall Defects
32 Reducing Damage to Alumina Fibers in Metal-Matrix Composites

Ceramic $Si_wB_xC_yO_z$ Fibers From Organic Si/B Polymer Precursors

Some of these fibers are stable at temperatures up to 1,300 °C.

Ames Research Center, Moffett Field, California

Improved formulations and processes have been invented for manufacturing ceramic fibers that exhibit structural stability and retain tensile strength at temperatures up to 1,200 °C, or even 1,300 °C in some cases. The final compositions of these fibers are given in the following table:

Element	Weight Percent
silicon	30 to 60
boron	2 to 8
carbon	18 to 40
oxygen*	<20

* Alternatively, as explained in the text below, fibers can contain nitrogen instead of oxygen.

These fibers are more stable at high temperatures than are the silicon carbide- and silicon nitride-based fibers made by the older processes described next.

Fibers containing the same elements in proportions different from those listed above have been made by older processes that involve (1) synthesis of precursor organic polymers, (2) extruding (melt-spinning) the polymer masses into fibers, and (3) treating the fibers by curing, sintering, and/or pyrolysis. In cases in which the polymer fibers are pyrolized directly, the fibers can deform or even melt during pyrolysis; this is a disadvantage in engineering applications in which fibers of specified shape are required.

The improved process includes the same basic steps as those described above. In addition, the improved process includes a step in which the precursor polymers are cured (their molecules are cross-linked) to prevent melting or deformation during the subsequent pyrolysis.

In a typical case, the improved process begins with heating a reaction mixture of an organoborohalide and an organohalosilane to synthesize a polyorganoborosilane, which is the precursor polymer. The polymer is then heated to a temperature between 80 and 200 °C (chosen to be somewhat above the softening or melting temperature of the polymer). The heated polymer is extruded into fibers by use of a standard spinneret, and the fibers are spun onto spools.

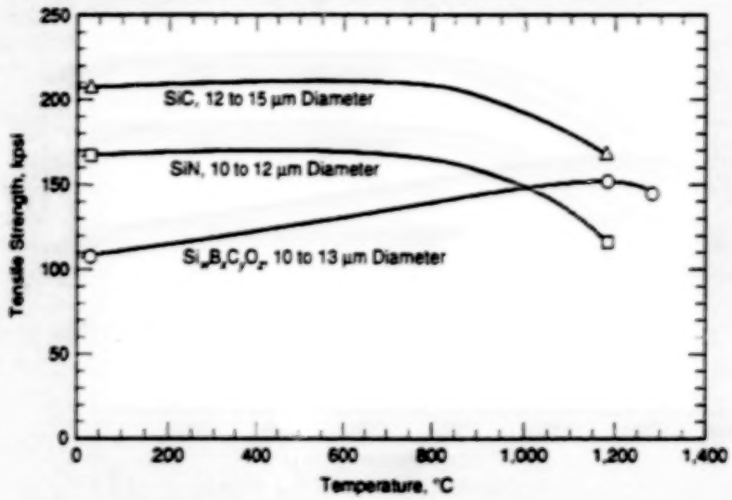

Tensile Tests Were Performed on representative fibers of this invention and of commercial SiC and SiN-based fibers. Unlike the other fibers, the fibers of this invention were found to grow stronger with increasing temperature up to about 1,200 °C.

The precursor polymer fibers are cured in one of following three ways:

- The fibers are oxidized slowly in air, starting at room temperature, gradually heating up to 150 °C during 3 or 4 days, and holding at 150 °C for about 1 day. Cross-linking is effected, and the level of oxygen incorporated in this step is between 5 and 25 weight percent.
- A better and faster oxidation-and-curing procedure involves irradiation of the fibers with ultraviolet light in air for 1 to 48 hours.
- A procedure for curing in the absence of oxygen involves exposure of the fibers to hydrazine vapor, preferably under a dry nitrogen or argon atmosphere for about 16 hours, followed by irradiation with ultraviolet light for 6 to 16 hours. In this procedure, nitrogen (instead of oxygen) is incorporated into the polymer.

The cured fibers are pyrolized by heating them from ambient temperature to about 1,300 °C in an inert atmosphere (argon or nitrogen). After initial heating, the fibers are held between 1,000 and 1,300 °C for as much as 1 hour. The products of pyrolysis are black fibers. The figure summarizes results of tensile tests of representative $Si_wB_xC_yO_z$ fibers made in this process and of commercial silicon carbide- and silicon nitride-based fibers, showing that the fibers of this invention retain tensile strength better at high temperature.

This work was done by Salvatore R. Riccitiello, Ming-ta S. Hsu, and Timothy S. Chen of **Ames Research Center**. *Further information is contained in a TSP [see page 1].*

This invention has been patented by NASA (U.S. Patent No. 5,223,461). Inquiries concerning nonexclusive or exclusive license for its commercial development should be addressed to the Patent Counsel, Ames Research Center [see page 1]. Refer to ARC-11956.

Tailoring Fiber/Matrix Interfaces Through Kirkendall Defects

Microporosity would be induced in thin interfacial layers.

John H. Glenn Research Center, Cleveland, Ohio

In a proposed method of tailoring some of the mechanical properties of metal-matrix, oxide-matrix, and ceramic-matrix composite materials, Kirkendall defects (microscopic pores as described below) would be introduced into thin interfacial layers between the fibers and the matrices. This method could be used in addition or as an alternative to an older method in which one seeks to tailor the mechanical properties of a composite by coating its fibers one or more layer(s) of material(s) distinct from the matrix and fiber materials.

The coatings of the older method are

applied as diffusion barriers to isolate the fibers from chemically reactive components of the matrix during processing or service, to protect the fibers from the effects of consolidation into the composite, to provide adequate bonding so that loads can be transferred from the matrix to the fibers, and/or to provide for deflection of cracks or for toughening the composite. In the case of multilayer coatings, each layer is applied in the effort to provide a beneficial effect that will contribute to the overall attainment of the protective effects listed in the preceding sentence.

In the proposed method, the fibers would be coated with an element that diffuses readily in the matrix material. Typically, such an element would be one that has a small atomic radius. The element must be one that is compatible with the matrix material at concentrations to be used.

Examples of techniques for depositing such elements include chemical vapor deposition (CVD), sputtering, and electron-beam physical vapor deposition (EB-PVD). During the thermal processing that is typically done to consolidate the composite, the coating material would diffuse away into the matrix as interstitial contaminants, leaving a porous interface behind. The resulting interfacial pores are instances of the classical metallurgical phenomenon known as "Kirkendall defects."

The initial coating and the subsequent porous interface would provide many of the protective effects mentioned above. In comparison with a composite that lacked the Kirkendall defects but was otherwise identical, the composite would be toughened because the porous interface would have a reduced cross-sectional area and would therefore be weaker.

The initial thickness of the diffusible coating, in conjunction with the processing parameters, would determine the extent of porosity created and, therefore, the degree of toughening. Other coatings could be applied either below or above the diffusible layer to further enhance the overall properties of the composite.

This work was done by Theodore R. Grossman of General Electric Co. for **Glenn Research Center**. *Further information is contained in a TSP [see page 1].*

Inquiries concerning rights for the commercial use of this invention should be addressed to NASA Glenn Research Center, Commercial Technology Office, Attn: Steve Fedor, Mail Stop 4–8, 21000 Brookpark Road, Cleveland, Ohio 44135. Refer to LEW-16733.

Reducing Damage to Alumina Fibers in Metal-Matrix Composites

Precoating the fibers by sputtering may increase the retention of strength.

John H. Glenn Research Center, Cleveland, Ohio

Coating alumina fibers with sputtered metal has been proposed as a means to enable the fibers to retain more strength when the fibers are incorporated into metal-matrix composites. If the alumina fibers could be made to retain more strength, then it would be possible to manufacture such composites with high volume fractions (20 to 40 volume) percent of fibers to obtain high-temperature properties suitable for such demanding applications as nozzles in engines of supersonic airplanes.

A metal-matrix composite of the type in question is formed by hot pressing or hot isostatic pressing of alumina fibers with a foil or powder of the metal that is destined to become the matrix. The issue of retention of strength arises because it has been observed, in the case of iron- and nickel-base alloy matrices, that the alumina fibers become degraded from their original strength of 425±25 kpsi (2.9±0.2 GPa) to mean strengths <150 kpsi (<1 GPa).

In preliminary experiments to test the proposed strengthening technique, alumina fibers were coated to a thickness of 4.7 μm by sputtering from a target of MA956 alloy. The coatings of some of the fibers were removed, and then the strengths of the fibers were measured and found to be about 360 kpsi (2.5 GPa). Other fibers were heated in a vacuum at a temperature of 1,200 °C prior to removal of coatings, and their strengths were found to be 310 kpsi (2.1 GPa). The sputtered coatings appeared to have resulted in only minimal strength-reducing damage to the fibers. Scanning electron micrographs of the fibers after removal of the coatings showed a surface appearance very different from that typically seen on fibers damaged by incorporation into metal-matrix composites.

Some caution in interpreting the observations in these experiments is in order, in part because the fibers were not rotated during sputtering and therefore the coatings did not extend around their entire circumferences. The fibers were also not coated along their full lengths. Moreover, it is not known whether the partial-strength-preserving effect of sputter coating is repeatable. Further experiments are planned to investigate the effects of full-circumference and full-length coating, to determine repeatability, and to learn more about the chemical and microstructural details of damaging versus nondamaging deposits. Another question to be addressed is whether alternative sputtering-target compositions and alternative coating processes could contribute to retention of strength.

This work was done by M. F. X. Gigliotti, Jr.; M. R. Jackson; and A. M. Ritter of General Electric Co. for **Glenn Research Center**. *Further information is contained in a TSP [see page 1].*

Inquiries concerning rights for the commercial use of this invention should be addressed to NASA Glenn Research Center, Commercial Technology Office, Attn: Steve Fedor, Mail Stop 4–8, 21000 Brookpark Road, Cleveland, Ohio 44135. Refer to LEW-16735.

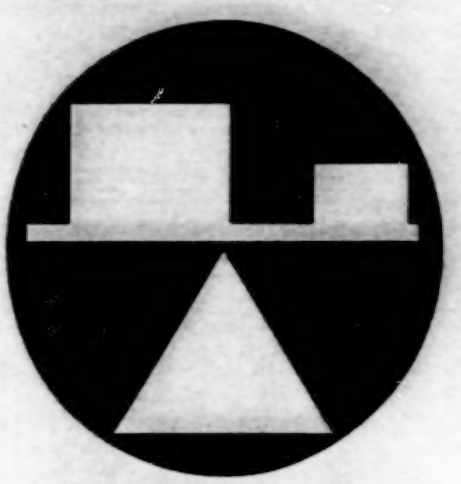

Mechanics

Hardware, Techniques, and Processes

35 Additive Beam for Modeling Dynamics of the SR-71 Fuselage
36 Composite-Fuselage Concept for Greater Crashworthiness
37 Five Computer Codes for Analysis of Turbomachinery
38 Software for Finite-Element Analysis of Thermoelasticity
39 A 3D Navier-Stokes CFD Code for Analysis of Turbomachinery

Books and Reports

39 Digital PIV Measurements of Flow in a Centrifugal Compressor
40 Low-Energy Interplanetary Transfers Using Lagrangian Points

Additive Beam for Modeling Dynamics of the SR-71 Fuselage

Computational simulations are more accurate.

Dryden Flight Research Center, Edwards, California

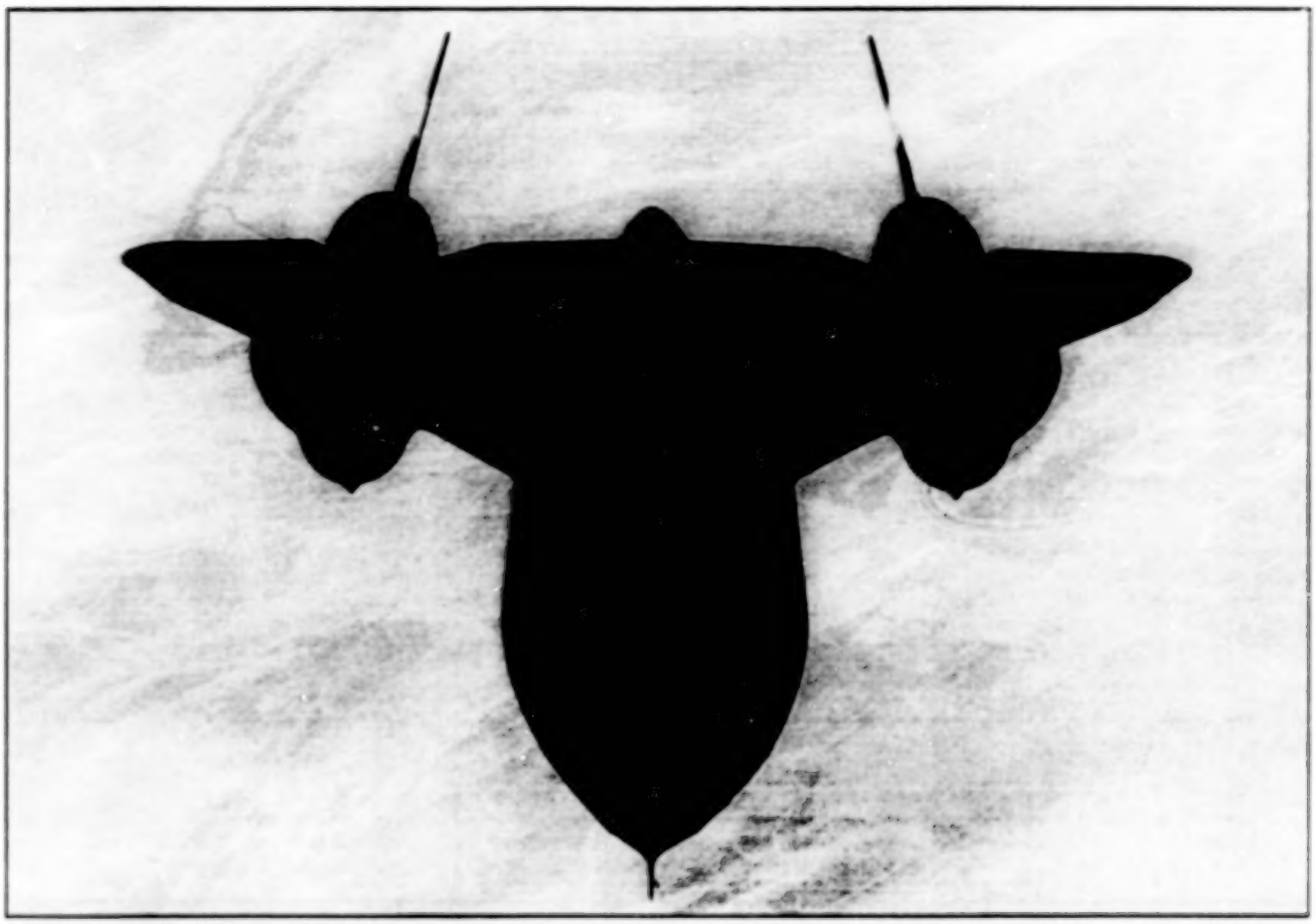

Figure 1. The **SR-71 Airplane** exhibits fuselage-bending vibrations that affect its overall dynamics and that must be taken into account to obtain accurate computational simulations of responses to pilot commands.

Mathematical models to approximate the dynamics of aircraft are often generated by considering aircraft structures to be rigid bodies. These models may be unsuitable for evaluating the maneuvering responses and flight characteristics of flexible aircraft. Computational simulations of the dynamics of a flexible aircraft by use of a model that does not account for the elasticity may indicate inaccurate tracking performance, handling qualities, and response bandwidth, especially in evaluations of responses to pilot commands.

It is necessary to account for the elastic as well as the rigid-body dynamics of the SR-71 airplane (see Figure 1) in order to simulate its overall dynamic responses accurately. In particular, a submodel of elastic dynamics must represent the first bending mode of the fuselage. This mode can significantly affect responses because large-amplitude oscillations in this mode are easily excited during standard pilot maneuvers. Thus, it is necessary to model

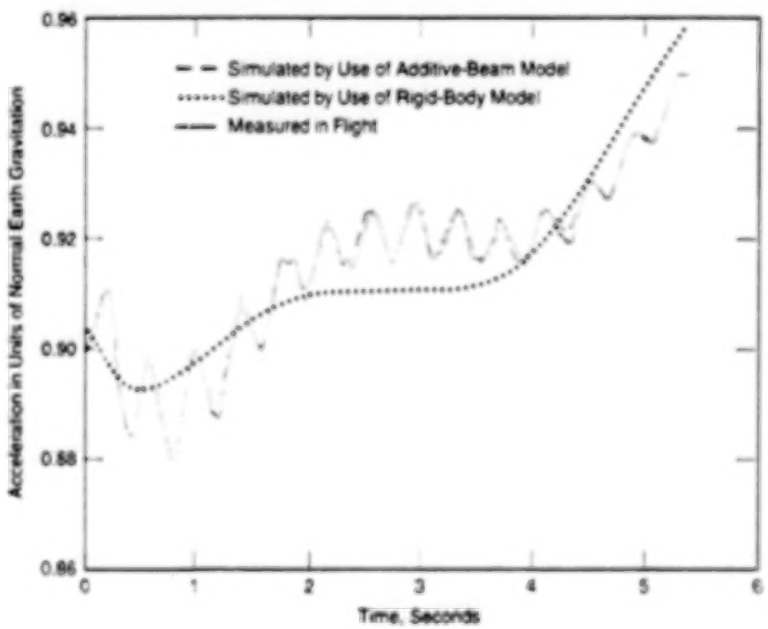

Figure 2. **Acceleration Near a Pilot Station** on the SR-71 airplane, in response to a pilot command, was measured in flight and simulated by use of two different mathematical models.

this mode accurately for closed-loop analysis and pilot simulations.

Flight data can be used to generate mathematical models that account for rigid-body and elastic dynamics, according to the method described in "Calibrating Aircraft-Vibration Models from Flight Data" (DRC-95-05), *NASA Tech Briefs*, Vol. 21, No. 11 (November 1997), page 78. In this method, one considers a general theoretical model and analyzes flight data by use of parameter-estimation algorithms to determine the optimal coefficients for that model. Models of the SR-71 airplane were developed by introducing a simple uniform beam to represent the mode shape of the fuselage in a general model. An optimal model resulting from analysis of flight data was found to be capable of simulating responses much more accurately than did rigid-body models; however, there were some errors in the simulated dynamics of the fuselage.

An additive-beam model has been conceived for use in representing the mode shapes of the elastic dynamics of the fuselage; in other words, the bending shapes of modes of vibration of the fuselage. This additive-beam model is formulated by superimposing the responses of a uniform beam with no fixed ends and a uniform beam with one fixed end. The resulting beam is not restricted to be symmetric about a midpoint and, consequently, can represent complex mode shapes.

A model of the SR-71 is generated by analyzing flight data according to the parameter-estimation method and utilizing a general model that includes the additive beam. Figure 2 presents an example of flight data — acceleration measured near the pilot station during a pitch maneuver — along with the corresponding simulated responses of a rigid-body model and the model that includes the additive-beam submodel. Responses from the additive-beam model are very similar to the flight data and are clearly more accurate than are the responses from the rigid-body model. Thus, the additive beam has been shown to represent accurately the first bending mode of the fuselage.

The additive beam is particularly useful for modeling the fuselage of the SR-71 because of the resulting complicated mode shape. This shape accounts for the variations in structural stiffness that occur along the fuselage as a result of wings and engine mountings. Similarly, additive-beam models can be included in models of other aircraft that have complicated mode shapes. For example, many long-endurance, high-altitude airplanes with long wing spans are affected by low-frequency bending modes with complicated mode shapes that cannot be accurately modeled by simple uniform beams.

This work was done by Rick Lind of **Dryden Flight Research Center** *and Carla Ioria of West Virginia University. Further information is contained in a TSP [see page 1].*
DRC-98-36

Composite-Fuselage Concept for Greater Crashworthiness

The fuselage is designed to protect occupants and absorb impact energy.

Langley Research Center, Hampton, Virginia

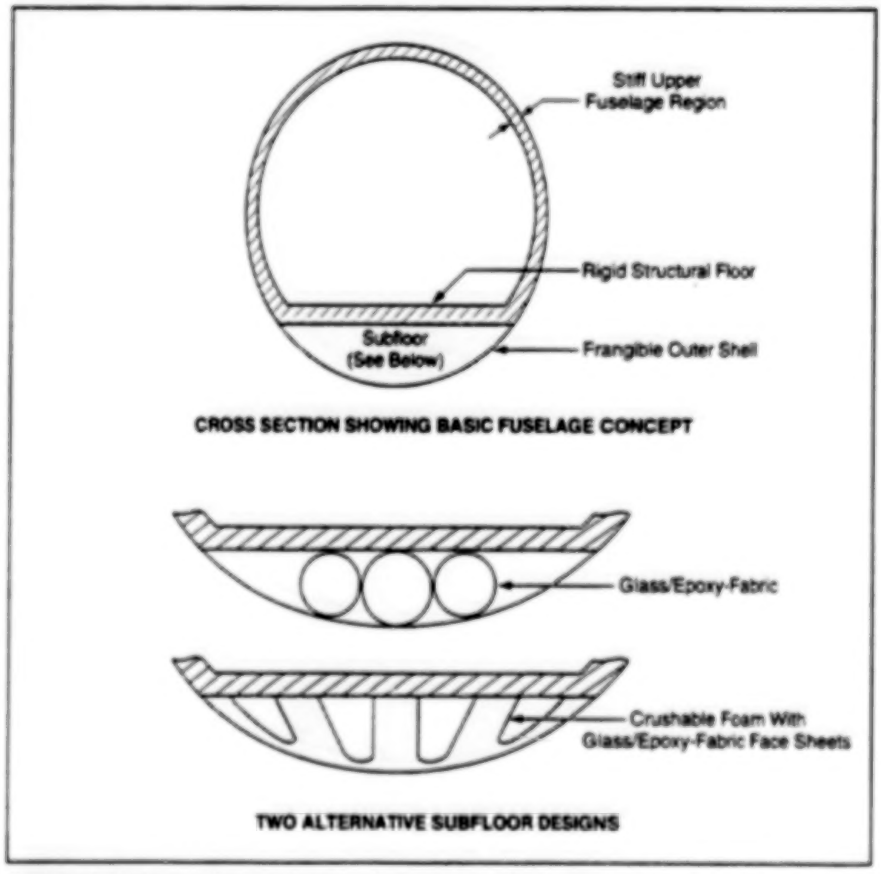

Different Regions of the Fuselage are designed to perform different roles to protect occupants during a crash.

A continuing program of research is directed toward the development of crashworthy composite-material fuselages for small aircraft. These fuselages are required not only to withstand flight loads and exhibit the required aerodynamic characteristics, but also to protect occupants during crashes more effectively than do conventional fuselages. The design goal for protection against crashes is to limit loads applied to occupants to survivable levels in vertical impacts onto rigid surfaces at a speed of 31 ft/s (9.4 m/s). This vertical impact speed exceeds that specified in current regulatory criteria for small aircraft, but it is a realistic, potentially survivable, impact velocity that has been observed in crashes and in crash tests performed at Langley Research Center.

The design concept that has emerged from this research calls for a structure made from several glass/epoxy-fabric and graphite/epoxy-fabric laminates plus some other materials. The fuselage is divided into four regions, as indicated in the figure. Each region is designed to satisfy a different set of requirements:

- The upper region is made of a stiff sandwich comprising a polyurethane foam core between glass/epoxy-fabric face sheets. This region is designed to

enclose and protect the occupants in the event of a crash.

- The outer shell is made from a relatively compliant glass/epoxy-fabric layer that is wrapped around the entire fuselage, enclosing an energy-absorbing structure (the subfloor) beneath a rigid structural floor. The outer shell is designed to have the required aerodynamic shape and to tolerate damage. The outer shell is intended to become deformed upon impact; this deformation, in turn, is intended to initiate crushing of the subfloor.
- The subfloor, described in more detail below, is designed to dissipate kinetic energy through stable crushing, and to maintain adequate post-crash structural integrity.
- The stiff structural floor is designed to react the loads generated by crushing of the subfloor, and to provide a stable platform for attachment of seats and restraints.

Two alternative subfloor designs have been selected: In one design, the main structural components of the subfloor are three laminated glass/epoxy-fabric tubes placed lengthwise along the fuselage. The sizes of the tubes, the number of layers of glass/epoxy fabric, and the orientations of the fibers in the layers must be chosen to optimize the absorption of energy by transverse crushing of the tubes upon impact.

In the other subfloor design, the space below the stiff structural floor is filled with closed-cell polymethylimide foam covered by glass/epoxy-fabric face sheets. The geometry of the foam subfloor was chosen to achieve and to maintain the desired crushing stress level.

The concept has been implemented in 1/5-scale models that have been evaluated in drop tests. The models were dropped from a height of 15 ft (4.6 m) to obtain vertical impact at a speed of 31 ft/s (9.4 m/s) onto a concrete surface. Floor-level accelerations of 125 times normal Earth gravitational acceleration (*g*) were obtained. (This impact requirement corresponds to a 25-*g* floor-level acceleration in a full-scale fuselage.) The data from the drop tests indicated that the model with a foam subfloor satisfied the impact design requirement. The results of a finite-element simulation of the impact behavior were found to be well correlated with the corresponding results from the drop tests.

This work was done by Karen E. Jackson and Edwin L. Fasanella of the Vehicle Technology Center of the U.S. Army Research Laboratory for **Langley Research Center**. *Further information is contained in a TSP [see page 1].*
L-17835

Five Computer Codes for Analysis of Turbomachinery

These codes can be used separately or else together in sequence.

John H. Glenn Research Center, Cleveland, Ohio

Figure 1. These Mach-Number Contours were computed for transonic flow around turbine vanes.

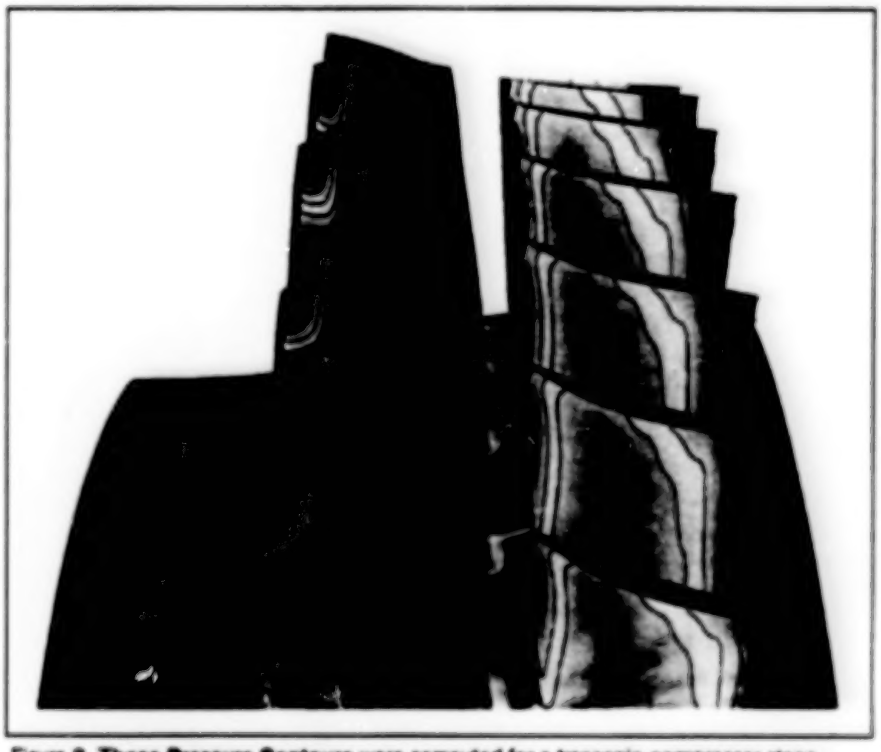

Figure 2. These Pressure Contours were computed for a transonic compressor stage.

A suite of five computational fluid dynamics (CFD) codes has been developed for analysis of flows in turbomachinery. Two of the codes are used to generate two-dimensional (2-D) or three-dimensional (3-D) grids that describe the turbomachinery blade geometry. The other three codes solve the Navier-Stokes equations on those grids to predict the performance of the blades. Three mathematical models of turbulence that include effects of flow transition and roughness are available. The codes are applicable to fans, compressors, and turbines in both axial and radial machines.

The codes include the following:

- GRAPE (Grids About Airfoils Using Poisson's Equation) generates a two-dimensional blade-to-blade periodic grid. GRAPE is used with RVCQ3D, which is described next.
- RVCQ3D (Rotor Viscous Code Quasi-3-D) is a code for quasi-3-D blade-to-blade analysis that includes the effects of rotation, change of radius, and vari-

able stream surface thickness.

- TCGRID (Turbomachinery C-Grid) generates a 3-D grid used with RVC3D and SWIFT, which are described next.
- RVC3D (Rotor Viscous Code 3-D) is a code for 3-D analysis of isolated blade rows.
- SWIFT is a code for 3-D, multiblock analysis that affords grid capabilities additional to those of RVC3D, including the ability to model tip-clearance flows and multistage turbomachinery.

The codes can be used independently but often are used in sequence. RVCQ3D is used to investigate many design parameters quickly in two dimensions, RVC3D is used to predict the performance of isolated blade rows, and SWIFT is used to study a 3-D blade in more detail or in a multistage environment.

RVCQ3D, RVC3D, and SWIFT solve finite-difference approximations of equations of flow by use of an explicit Runge-Kutta scheme. A spatially variable time step and implicit residual smoothing are used to accelerate convergence. Preconditioning can also be performed for low-speed (incompressible) flows.

The codes have been verified with respect to transonic flow around turbine vanes (see Figure 1) and with respect to a transonic compressor stage (see Figure 2). They have also been used to analyze many fan blades, the fuel turbine for the space shuttle main engine, wind-tunnel turning vanes, centrifugal compressors, and a vacuum-cleaner impeller.

The codes are written in Fortran and can be compiled and run on most computers. Blade data are entered by use of a common Glenn Research Center design-code format. Simple namelist input is used for flow parameters. Some printed output is generated. No graphical output is provided, but grid and solution files are in a standard format that can be read directly by most CFD visualization software packages, including FAST and PLOT3D.

This work was done by Rod Chima of **Glenn Research Center**. *Details about the individual codes and sample results may be found on the author's web site,* ***www.grc.nasa.gov/WWW/5810/webpage/rvc.htm***. *Further information is contained in a TSP [see page 1].*

LEW-16851

Software for Finite-Element Analysis of Thermoelasticity

This program utilizes p-version finite elements for accuracy in resolving gradients.

Lyndon B. Johnson Space Center, Houston, Texas

The P-Finite Element Integrated Thermal-Structural Program (PITS 2D) solves the equations for the combined effects of thermal expansion and elasticity in a two-dimensional or an axisymmetric three-dimensional structure. The name of this program reflects the use of *p*-version finite elements, in contradiction to the traditional use of *h*-version finite elements. In comparison with older finite-element programs that utilize the *h*-version, PITS 2D predicts physical response more accurately in the presence of large gradients.

A *p*-version finite element in PITS 2D (see figure) can be either a quadrilateral or a triangle with concave and/or convex curved sides. A quadrilateral element is defined by eight nodes: four of them define the corners, and each of the remaining four nodes defines the approximate midpoint of a curved side. Similarly, a triangular element is defined by six nodes, three lying at the corners and each of the three remaining nodes lying at about the midpoint of a curved side.

In an *h*-version finite element, the displacements, stresses, strains, temperature, and other physical quantities are represented by trial first-order functions of spatial coordinates. The solution that one seeks is embodied in the coefficients of the functions. In a *p*-version finite element, the physical quantities are represented by polynomials that can be of orders higher than first. Thus, the polynomials of the *p*-version can fit physical data points more smoothly and accurately than can the linear functions of the *h*-version. In a given case, the error in the solution can be made smaller by using a polynomial of higher order. In PITS 2D, the polynomials can be of any order from first to eighth.

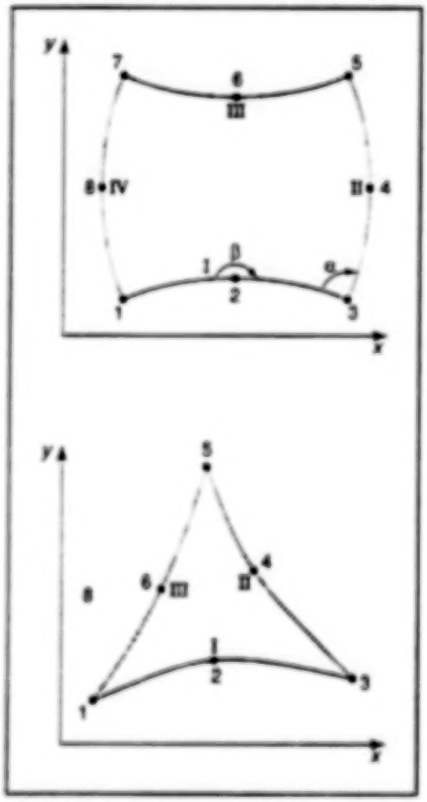

Eight-Node Quadrilateral and six-node triangular finite elements are used in PITS 2D.

Examples of phenomena that can be analyzed by use of the current version of PITS 2D include stresses and/or temperatures in two-dimensional or axisymmetric three-dimensional structures made of isotropic or orthotropic materials, bending and buckling in thick plates made of isotropic or orthotropic materials, torsion in beams, and potential flow of fluid around a body. Nonlinear effects of thermal radiation (without stress) can be analyzed in cases of isotropy or orthotropy; nonlinear effects of thermal radiation (with stress) can be analyzed in cases of isotropy. Boundary conditions on displacement, stress, temperature, thermal flux, and convection can include quadratic spatial variations.

PITS 2D is based largely on an older finite-element program called "BUCKY." It was developed and tested on computers running the Linux, HP-UX, and SunOS operating systems. A standard Unix Fortran 77 compiler and linker are necessary for execution.

This work was done by James P. Smith of **Johnson Space Center**. *Further information is contained in a TSP [see page 1].*

MSC-22832

A 3D Navier-Stokes CFD Code for Analysis of Turbomachinery

This code can be used to model complex, multiple-path flows.

John H. Glenn Research Center, Cleveland, Ohio

The ADPAC software is a computational fluid dynamics (CFD) code for analysis of flows in turbomachines. The outstanding feature of ADPAC is the ability to solve the Navier-Stokes equations for complex three-dimensional (3D) flow fields that include multiple flow paths, and the modeling of which typically involves multiple computational grid blocks. In addition, ADPAC can handle coupled calculations in which some portions of models are rotating and some are not, as in the case of the rotating blades and stationary vanes of a turbomachine. ADPAC was developed especially for use in analyzing the performances of short-duct, ultrahigh-bypass-ratio turbofan engines, both as uninstalled and as installed; however, ADPAC is applicable to a very broad range of other turbomachines and of other flow systems.

There are now several commercially available computer programs that offer capabilities similar to those of ADPAC. However, when the development of ADPAC began (circa 1989) 3-D Navier-Stokes CFD codes for turbomachinery could handle only single flow paths, and only a few codes could handle more than one component at a time. NASA had a need for a CFD code that could simultaneously handle multiple flow paths (through the core, through the bypass duct, and outside the cowl), multiple blade rows, and tightly coupled components of conceptual ultrahigh-bypass-ratio turbofan engines. Prior to the development of ADPAC, computational simulations of such complex flow fields were done in parts: In a typical case, each flow path and each blade row was split out, gridded, and run separately. Then the data at the interfaces between blocks were adjusted and the individual blocks run again until there was convergence. This decoupled-solution method proved to be inefficient and time-consuming.

The development of ADPAC involved rewriting of a prior 3D, viscous-flow CFD code that was capable of handling a single flow path with a single grid block. The rewriting included the incorporation of multiblock and multigrid capability, extra boundary conditions, and mathematical models of turbulence. The resulting ADPAC code is characterized by the following major features and capabilities:

- *External Inflow*: On-axis or off-axis for configurations at various angles of attack.
- *Internal Inlet*: Uniform (or plug) flow; distortion patterns with mixed radial and circumferential distributions of total pressure and total temperature.
- *Boundary Conditions*: Solid walls bounding inviscid or viscous flow; porous walls with inflow or outflow; and exit planes with constant static pressure or radial equilibrium.
- *Grids*: Multiple blocks; mixed C, H, I, and/or O grids (with some restrictions); mixed axisymmetric and/or three-dimensional grids with single or multiple blade passages; and multiblock binary (Cartesian) grids stored externally as PLOT3D files.
- *Coupling Among Blocks*: All boundary conditions must be given on a common face. Direct patch or interpolation is possible for mismatched grids with no relative movement. Mixing-plane or unsteady interpolation is possible for blocks with relative movement.
- *Block Periodicity*: Cylindrical (as for turbomachinery) or Cartesian (as for linear cascades or aircraft).
- *Flow Paths*: Multiple.
- *Solver Algorithm*: Finite-volume 4- or 5-stage Runge-Kutta explicit, dual time step implicit, multigrid acceleration, parallelized via message passing, APPL, PVM, or MPI libraries.
- *Turbulence Models*: Baldwin-Lomax with wall functions, restricted to the block with the wall; Goldberg's k-R; and Spalart-Allmaras.
- *Time-Marching Throughflow Capability*: Turbomachinery blade rows represented as 2-D axisymmetric surfaces with body forces to represent flow turning and profile losses.
- *Inverse Design Capability*: Turbomachinery blade row design based on time-marching throughflow simulation with user-specified tangential velocity and airfoil thickness distributions.

This work was done by Christopher J. Miller of **Glenn Research Center** *and Edward J. Hall, Nathan J. Heidegger, Michael L. Koiro, and David A. Topp of Rolls Royce Allison Engine Division. Further information is contained in a TSP [see page 1].*

LEW-16768

Books and Reports

Digital PIV Measurements of Flow in a Centrifugal Compressor

A report describes experiments in which digital particle-image velocimetry (digital PIV) was used to measure the flow field in the diffuser of a high-speed centrifugal compressor. In digital PIV, a sheet of pulsed laser light illuminates a flow field seeded with small tracer particles, the positions of the particles are recorded on a digital charge-coupled-device (CCD) camera at each pulse time, and the digitized image data are processed to extract velocities from the displacements of particles between pulses. In the experiments, a special periscope probe was used to introduce the light sheet into the flow plane of interest inside the compressor, and a CCD camera was mounted on the outside of the compressor to monitor the plane of interest via a mirror and a window. Measurements were obtained while the compressor ran at design speed, yielding highly accurate time-averaged velocity-vector maps in much less time than is needed to generate comparable maps by use of laser Doppler velocimetry (LDV). It was shown that by use of PIV, measurements could be taken closer to the compressor-hub surface than was possible using LDV. The report also presents initial results from PIV measurements of unsteady flow during compressor surge.

This work was done by Mark P. Wernet of **Glenn Research Center**. *To obtain a copy of the report, "Digital PIV Measurements in the Diffuser of a High Speed Centrifugal Compressor," see TSP's [page 1].*

Inquiries concerning rights for the commercial use of this invention should be addressed to NASA Glenn Research Center, Commercial Technology Office, Attn: Steve Fedor, Mail Stop 4–8, 21000 Brookpark Road, Cleveland, Ohio 44135. Refer to LEW-16878.

Low-Energy Interplanetary Transfers Using Lagrangian Points

A paper summarizes early findings from a continuing study of the dynamics of the transport and distribution of matter within the Solar system. In the study, the stable and unstable manifolds of the periodic and quasi-periodic orbits around the Lagrangian points L1 and L2 of the Sun/planet and planet/Moon subsystems are found to play an important role. (The Lagrangian points are five points, located in the orbital plane of two massive bodies, where a much less massive body can remain in equilibrium relative to the massive bodies.) The formulation of dynamics in terms of these manifolds is found to explain how a Kuiper Belt object can be transported to become a Jupiter comet, eventually evolving into an asteroid that could reach the inner Solar system. The same formulation of dynamics could be exploited to obtain low-energy interplanetary spacecraft trajectories and captures. The fruits of the study could even include means to identify dangerous asteroids on collision courses with Earth, and low-energy strategies for deflecting them onto safer trajectories.

This work was done by Martin Lo and Shane Ross of Caltech for **NASA's Jet Propulsion Laboratory**. *To obtain a copy of the paper, "Low Energy Interplanetary Transfers Using the Invariant Manifolds of L1, L2, and Halo Orbits," see TSP's [page 1].*
NPO-20377

Machinery

Hardware, Techniques, and Processes

43 Force-Reflecting, Finger-Position-Sensing Mechanism
44 Insectile and Vermiform Exploratory Robots
45 Better Densification of Cryogenic Liquid Rocket Propellants
46 Robot Would Inspect Hanging Cables

Force-Reflecting, Finger-Position-Sensing Mechanism

This exoskeletal device is part of a hand-operated apparatus for controlling a robotic manipulator.

Lyndon B. Johnson Space Center, Houston, Texas

An electromechanical device called the "Dexterous Master" (DM) is an exoskeletal mechanism that is worn on a human operator's hand for (1) measuring the positions and orientations of the fingers relative to the palm and (2) applying, to the fingers, feedback forces from a remote robotic manipulator. The DM is part of a force-reflecting, hand-operated control apparatus through which the operator controls the manipulator. The DM is installed on, and operated in conjunction with, another mechanism that measures the position and orientation of the hand and reflects forces to the hand in the six degrees of freedom that determine the position and orientation of an end effector (robot hand) on the manipulator.

The DM has nine passive parallel degrees of freedom (DOFs) and six actuated parallel DOFs. It includes five finger assemblies, which are mounted on the dorsal surface of the hand to minimize the probability of collisions among fingers and mechanisms. The design of the finger assemblies is based on the proposition that it suffices to measure the position and orientation of each fingertip, with no need to measure the angles of the joints between the fingertip and the palm; this proposition makes it unnecessary to encumber each finger joint with hardware.

A control computer calculates real-time coordinate transformations between (1) the positions and orientations of the operator's fingertips and (2) the positions and orientations of fingertips or other corresponding parts on the robotic end effector. This control scheme renders master/slave kinematic similarity unnecessary, thereby enabling the slaving of a variety of multilink robotic arms and hands.

The six actuated DOFs (two for the thumb, one for each of the other four fingers) are implemented by use of six identical servo-controlled actuator units. The actuators are small electric brushless motors connected to synchronous belt-drive trains.

With the exception of the thumb, each finger assembly includes one actuated revolute joint (ARJ), one passive prismatic joint (PPJ), and a passive revolute joint (see figure). The thumb assembly is similar except that it includes two ARJs. The particular revolute/prismatic arrangement was chosen primarily because it offers an optimum solution to the problem of transducing the position of three DOFs per finger while actuating only one.

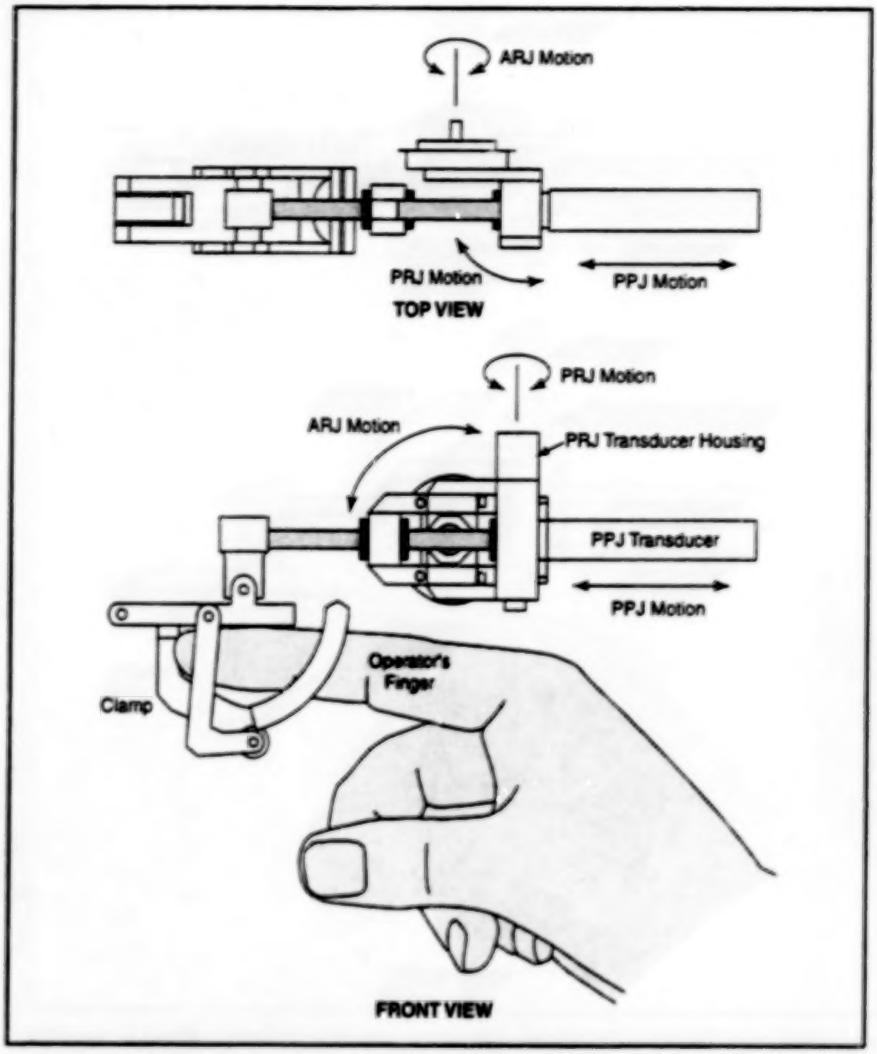

A Finger Assembly contains joints and joint transducers that allow natural finger motion and measure the position and orientation of the fingertip.

Each ARJ consists of the bull gear from one of the synchronous belt-drive trains and a radial ball-bearing set. Each PPJ consists of a length of a steel slider bar in a linear recirculating-ball-bearing set. Each PRJ consists of a radial ball-bearing set; it allows revolute motion of the slider bar about an axis perpendicular to both its axis of linear travel and the axis of the actuated revolute joint. The motion of an ARJ (other than the second thumb ARJ) corresponds approximately to the inclination/declination of the proximal joint of the affected finger. The motion of a PPJ corresponds approximately to extension/retraction of the tip of the affected finger with respect to the palm. The motion of a PRJ corresponds approximately to adduction/abduction of the affected finger.

The position of a slider rod along a PPJ is transduced by a linear variable-differential transformer (LVDT) in which the slider bar serves as the transformer core. The angle of a PRJ is measured by a shrouded light-emitting-diode/photoreceptor pair aimed at a rotary polytetrafluoroethylene target. The angle of an ARJ is measured by use of a shaft-angle encoder on its motor. The ARJ, PPJ, and PRJ, through their respective transducers, together provide sufficient data to define the location of the fingertip in spherical coordinates. At the same time, servoing the motor presents the required haptic feedback to the fingertip. Separate actuation of the sliding rod is unnecessary because when the gear is held in place by the application of torque, the sliding rod is positioned so that it cannot be slid freely along its path without a very unnatural motion of the finger.

The tip of each finger assembly is equipped with a mechanism designed specifically for clamping the fingertip. The finger clamp is sprung closed, and a cam action is used to ensure effective clamping while accommodating a large variance in operator finger sizes. The DM superstructure is held stationary, relative to the palm, by means of a fingerless glove with hook-and-loop straps for donning and doffing.

This work was done by Vikas K. Sinha, Eric W. Endsley, Alan J. Riggs, and Brian K. Millspaugh of Cybernet Systems Corp. for **Johnson Space Center**. *MSC-22846*

Insectile and Vermiform Exploratory Robots

These robots would carry sensors in hazardous environments.

NASA's Jet Propulsion Laboratory, Pasadena, California

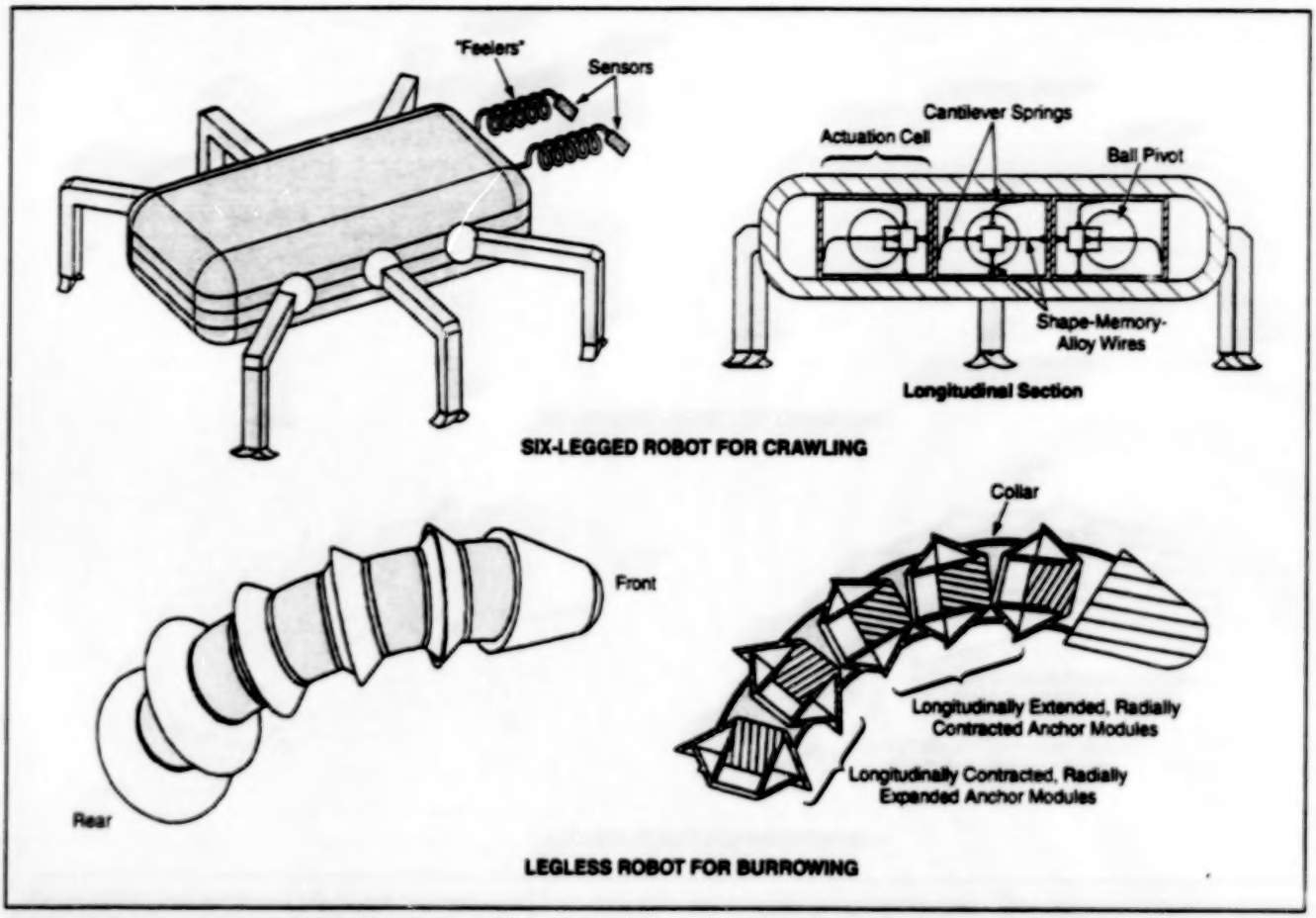

Robots That Look and Move Like Small Animals would be developed for use in a variety of exploratory tasks. Six-legged robots could be developed into a mass-producible, mass-deployable units to search for antipersonnel mines. Legless robots similar to the one depicted here could burrow in earthquake rubble to search for survivors.

A six-legged robot resembling an insect and a legless segmented robot resembling a worm (see figure) have been proposed as prototypes of biomorphic explorers — small, mobile, exploratory robots that would be equipped with microsensors and would feature animallike adaptability and mobility. Biomorphic explorers and related concepts have been described in several previous articles in *NASA Tech Briefs*, the most relevant being "Biomorphic Explorers" (NPO-20142), Vol. 22, No. 9, (September 1998), page 71 and "Earthwormlike Exploratory Robots" (NPO-20266), Vol. 22, No. 6, (June 1998), page 11b.

Depending on the specific environment to be explored, a biomorphic explorer might be designed to crawl, hop, slither, burrow, swim, or fly. Biomorphic explorers could be used for such diverse purposes as scientific exploration of volcanoes, law-enforcement surveillance, or microsurgery. Another potential use for biomorphic explorers is detection of antipersonnel mines; there is a pressing need for robots that could be deployed in large numbers to detect antipersonnel mines left on and in the ground after armed conflicts. The proposed six-legged robot would be designed with a view toward that application. There is also a need for burrowing robots that could search earthquake rubble for survivors; the proposed vermiform robot would be suitable for this purpose.

The proposed six-legged robot would be capable of traversing various types of terrain. The legs would be attached to a main body at shoulder ball pivots. Rotations at the shoulders would result in translations of the feet. The legs would feature telescoping segments that could be lengthened or shortened to suit the direction of motion and the terrain. For example, the legs could be shortened to obtain greater mechanical advantage for climbing, or lengthened to increase speed in level or downhill travel over smooth terrain. The legs would be tipped with footpads that could be config-

ured to suit the terrain. For example, a scissorlike arrangement of footpad members would be use on hard terrain (e.g., rocks), while the footpad members would be spread out to form a larger contact area on soft terrain (e.g., sand). The legs and footpads would be actuated by springs paired with shape-memory-alloy (SMA) wires; within each actuator, the spring would pull or push in one direction, while the SMA wire would pull in the opposite direction by an amount that would be changed momentarily by passing a momentary electric current through the wire to heat it momentarily above its shape-memory transition temperature.

The proposed vermiform robot would be capable of both anchored rectilinear motion similar to peristalsis and a transverse motion, based on the motions of *Amphisbaenia* — a legless order of reptiles that burrow with notable efficiency. The anchored rectilinear motion would be effected by anchor modules that would look like cones paired base to base. Within each anchor module there would be a pistonlike assembly actuated by pairs of springs and SMA wires. The assembly could be actuated to either (1) shorten the module longitudinally and expand the outer cone radially to anchor in the wall of the burrow or (2) lengthen the module longitudinally and retract the outer cone from contact with the tunnel wall. For example, suppose that all anchor modules were initially in the minimum-diameter, maximum-longitudinal-length configuration. The foremost module could be expanded radially to anchor the head end, then the next module could be expanded, and so forth, in sequence from front to rear. The longitudinal shortening accompanying the radial expansion of each module would draw the trailing modules forward.

The anchor modules would be connected by collars of a flexible material in which SMA wires would be embedded at multiple circumferential positions. The SMA wires would be oriented longitudinally. The wires could be energized selectively to bend the collar; in this way, part or all of the robot body could be arched.

In both robots, artificial neural networks would receive inputs from sensors and would respond by issuing commands for the SMA actuators to effect complex combinations of motions to achieve the overall lifelike mobility. Artificial neural networks were chosen for this application because they appear to offer the maximum potential for achieving a desired combination of capability for learning, adaptability, fault tolerance, composability (ability to smoothly integrate various primitive motions into complex motions and other activities), and generality to enable application to future biomorphic explorers.

This work was done by Sarita Thakoor, Brett Kennedy, and Anil Thakoor of Caltech for **NASA's Jet Propulsion Laboratory**. *Further information is contained in a TSP [see page 1].*
NPO-20381

Better Densification of Cryogenic Liquid Rocket Propellants

Supercooling would enable reductions of size and weight.

Lyndon B. Johnson Space Center, Houston, Texas

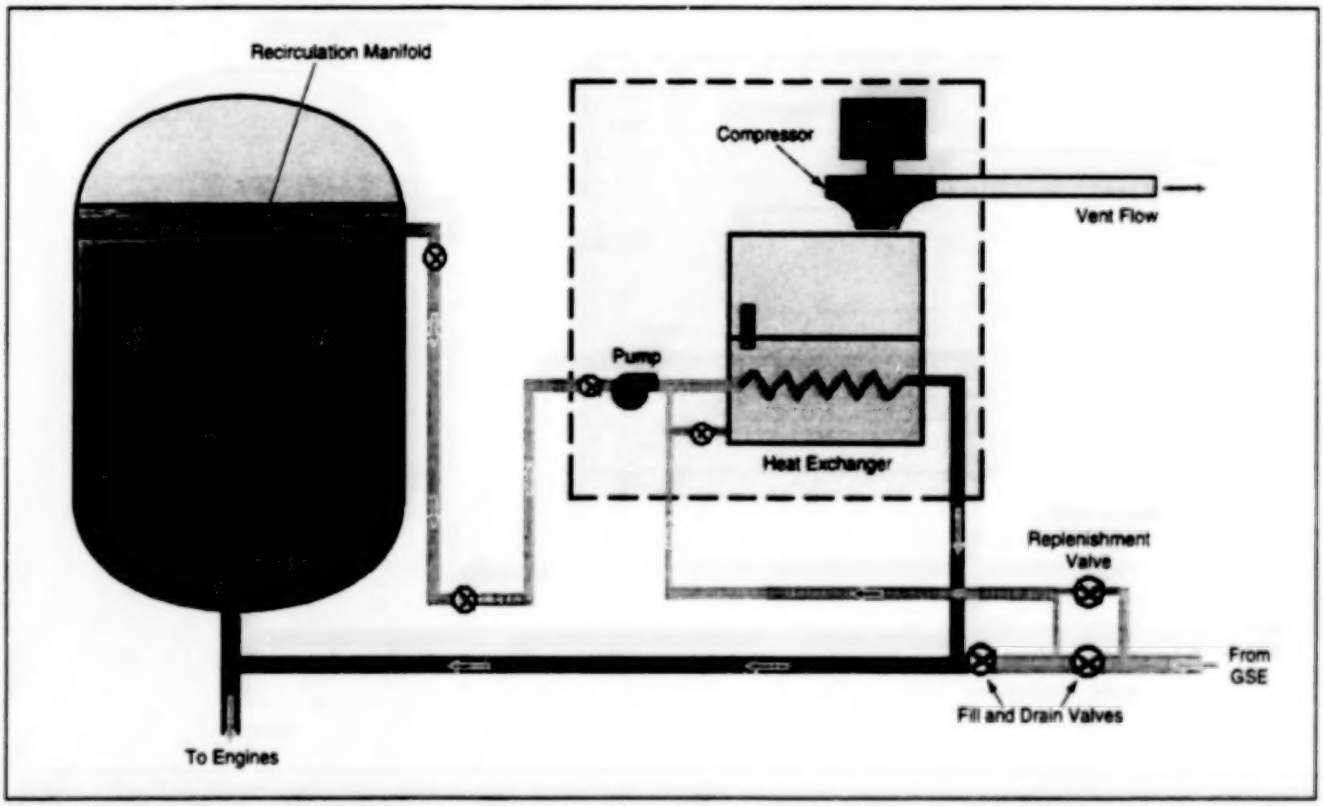

Figure 1. The **Tank Recirculation Subsystem** would continuously circulate the warmer cryogenic propellant liquid from the tank along with a supercooled stream of the same liquid.

An improved system for densifying (by cooling) the liquid hydrogen and liquid oxygen used as propellants for the space shuttle has been proposed. These propellant liquids are cooled to minimize the sizes of tanks needed to store them and to reduce maximum operating pressures. The proposed system would densify these liquids 7 to 8 percent more efficiently than does the

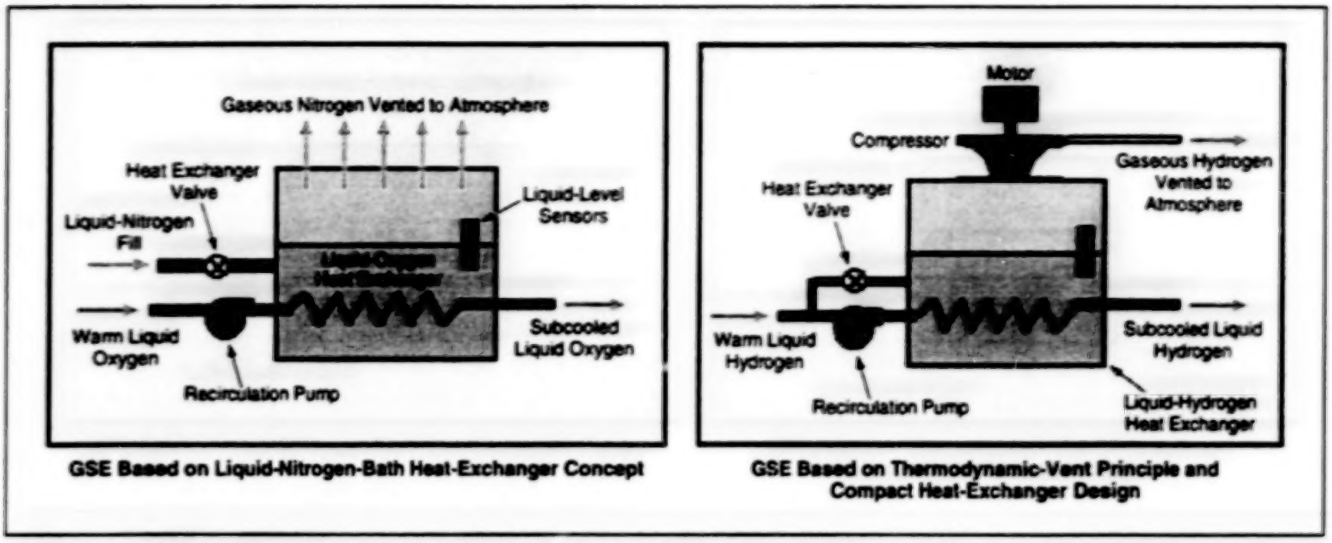

GSE Based on Liquid-Nitrogen-Bath Heat-Exchanger Concept

GSE Based on Thermodynamic-Vent Principle and Compact Heat-Exchanger Design

Figure 2. The **GSE Cooling Unit** would vent heat and keep the propellant liquid subcooled. The GSE unit could be designed according to a heat-exchanger-bath concept or a thermodynamic-vent principle.

present propellant-densification system, and would reduce the absolute vapor pressure from about 15 psi (≈0.1 MPa) to about 1.5 psi (≈10 kPa). Sizing analysis indicates that the combination of the increase in density and the decrease in vapor pressure would reduce the weight of the space shuttle by 10 to 20 percent. Similar reductions in the required volumes and weights of tanks for storing cryogenic liquids could be beneficial in any industry in which the sizes of such tanks are cost factors.

Densification of the space-shuttle propellant liquids is done during stable replenishing operations. Heretofore, these liquids have been cooled through surface-evaporation heat transfer and convective mixing. This method of cooling, while simple, is time-consuming and constrains the tank pressure to one atmosphere (≈0.1 MPa). The proposed system — a product of research at Rockwell International — would supercool the liquids to lower temperatures and vapor pressures than does the present system, and in a fraction of the time. An added advantage of the proposed system is that a vent valve would be relocated from the flight vehicle to the ground, with consequent further reduction in vehicle weight and simplification of design.

The proposed system (more precisely, a pair of systems — one for each liquid) would comprise two subsystems: (1) a tank recirculation subsystem (see Figure 1), which would continuously recirculate the initially warm liquid in the affected propellant tanks with subcooled liquid; and (2) a ground support equipment (GSE) cooling unit (see Figure 2), which would vent heat and keep the liquid subcooled. The GSE unit could be designed in one of two ways: as a simple heat exchanger or based on the thermodynamic-vent principle. The heat-exchanger design would involve use of a liquid bath as a boiling liquid medium. In the thermodynamic-vent version, a fraction of the recirculation fluid would be expanded to a lower pressure without changing its internal heat content. This throttling of the liquid, or moving from high pressure to low pressure, would cause the liquid to flash to a low temperature. The flashing, in turn, would cool the recirculating fluid. The low pressure on the colder side of the heat exchanger would be maintained by a compressor/blower unit, which would reject the vented gas from the low pressure to ambient pressure.

The GSE design would be determined by the thermodynamic properties of the liquid being recirculated and by cost constraints. The heat-exchanger GSE design, while less effective, would be less costly to build, especially for a fixed-structure system like the space shuttle. The thermodynamic-vent GSE design would be most beneficial in a new system because the vehicle could be designed according to the reduced volume and weight requirements associated with the improved cooling system.

This work was done by Tibor I. Lak, Steve P. Petrila, and Martin E. Lozano of Rockwell International for **Johnson Space Center.**

Title to this invention has been waived under the provisions of the National Aeronautics and Space Act [42 USC 2457 (f)], to The Boeing Co. Inquiries concerning licenses for its commercial development should be addressed to

Danielle Bartoli
The Boeing Co.
Canoga Park, CA 91309-7922
Tel. No. (818) 586-1367

Refer to MSC-22723, volume and number of this NASA Tech Briefs *issue, and the page number.*

Robot Would Inspect Hanging Cables

A proposed automated apparatus would travel along a hanging cable, optically inspecting it all around. The proposal was made to eliminate lowering human inspectors in baskets along emergency-egress slidewires at Kennedy Space Center launch pads. The apparatus would include a motor drive system, a video camera configured with mirrors for a 360° view of the cable, a data-capturing system, a laser micrometer, a video transmitter, and a radio transceiver for command and data signals. The apparatus would be placed on a cable at one end, then the inspection process would be initiated. During the process, the apparatus would operate under the control of a compact, rugged, onboard computer. Upon reaching the far end of the cable, the apparatus would automatically reverse itself and return to the starting end. An electronic neural network could be used, either on board the apparatus or in the command station, to analyze the

inspection data to determine the integrity of the cable.

This work was done by Robert L. Morrison, Kenneth M. Nowak, Terence J. Ross, Eduardo Lopez del Castillo, Michael D. Hogue, and Tom Bonner of and Gabor Tamasi formerly of **Kennedy Space Center**.

This invention is owned by NASA, and a patent application has been filed. Inquiries concerning nonexclusive or exclusive license for its commercial development should be addressed to the Technology Programs and Commercialization Office, Kennedy Space Center, (407) 867-6373, or for information regarding commercially available application of this technology contact: Halkin International at Halkin!@aol.com or telephone (303)344-9592 (a nonexclusive licensee). Refer to KSC-12023.

Mathematics and Information Sciences

Hardware, Techniques, and Processes

51 Software for Creating Real-Time Monitoring Expert Systems

Software for Creating Real-Time Monitoring Expert Systems

An expert-system developer need not write any program code.

Goddard Space Flight Center, Greenbelt, Maryland

The Generic Spacecraft Analyst Assistant (GenSAA) computer program enables the rapid development of expert-system software for intelligent real-time monitoring and detection of faults in complex systems of hardware and software. The hardware/software systems to which GenSAA expert systems were originally intended to be applied are spacecraft-control centers that feature the Transportable Payload Operations Center (TPOCC) architecture, which is a Unix-based architecture used at Goddard Space Flight Center. An expert system built by use of GenSAA is a rule-based system that assists spacecraft analysts during operation of a control center; the expert system receives spacecraft telemetric and ground-system-status data, makes inferences and draws conclusions about the data, and generates textual and graphical displays of the data and the conclusions. Continuing development of GenSAA includes generalization of its capabilities to build expert systems for non-TPOCC control centers and for non-spacecraft-control applications, which could include industrial process control, monitoring of networks, and monitoring and control of vehicular traffic.

GenSAA serves as an alternative to commercial expert-system-development software tools, which generally require programming skills beyond those of typical domain experts (human spacecraft analysts in the original intended applications). The effort involved in the use of such tools constitutes an impediment to the rapid development of the desired expert-system software. GenSAA overcomes this impediment, making it possible for domain experts without advanced programming skills to develop monitoring, graphical-display expert systems.

GenSAA comprises (1) the GenSAA Workbench, which is an integrated set of utility subprograms; and (2) the GenSAA Runtime Framework, which is a run-time executive subprogram. The GenSAA Workbench generates a graphical user interface (GUI) that enables the development of an expert system by use of point-and-click and drag-and-drop actions; it is not necessary for the expert-system developer to write any expert-system program code. The expert-system developer uses the Workbench for laying out the GUI of the expert system, defining fault-detection rules, and selecting the telemetry data to drive the expert system. GenSAA insulates the developer from the complicated programming details of the data source (e.g., the spacecraft ground system) and the GUI.

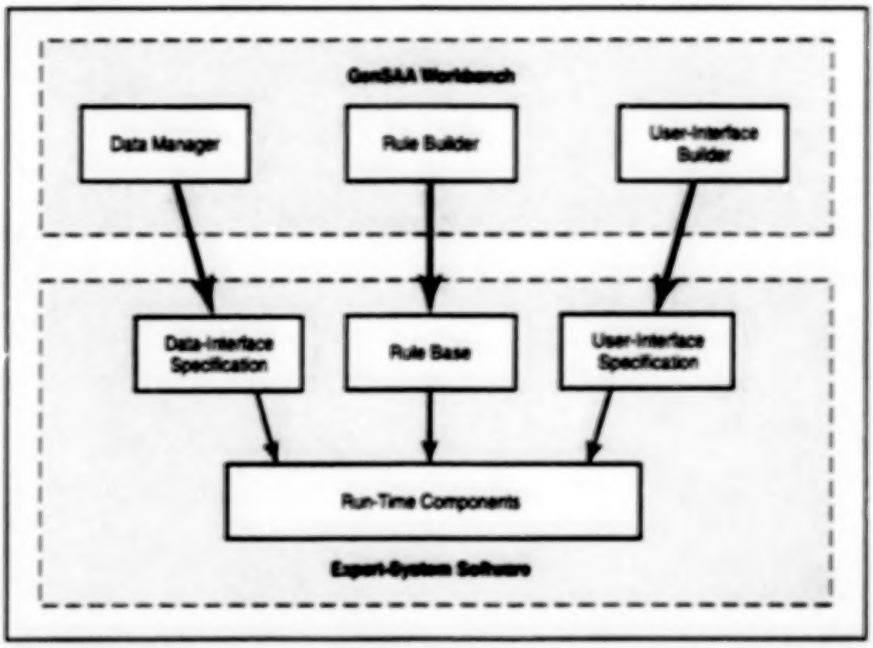

Three Utility Subprograms in the GenSAA Workbench are used to create a data-interface-specification file, a rule-base file, and a user-interface-specification file; these files are later be used by the GenSAA run-time framework to define an executable expert system.

The utility subprograms of the GenSAA Workbench are the following:

- Data Manager — This program is used to construct and edit four types of variables that are used by a GenSAA expert system. All variables that will be received from external data sources, exchanged with other GenSAA expert systems, or associated with GenSAA graphical objects must be specified by use of the Data Manager.
- Rule Builder — This program is used to create the rule base for an expert system. The rule base is a group of rules in "condition-action" ("if - then") format that may infer new facts based on currently asserted facts. A rule contains one or more conditions and one or more actions. An inference engine manages the matching and firing of rules in the rule base during execution of the GenSAA expert system.
- User Interface Builder — This is a powerful tool for creating GUIs. The user interface of a GenSAA expert system consists of a workspace, graphic windows, and graphic objects. These graphical elements can be dynamically created and customized, without programming, by use of mechanisms provided in the User Interface Builder.

The GenSAA Workbench creates a set of files that are used by the GenSAA Runtime Framework (see figure) to define the executable GenSAA expert system. The GenSAA Runtime Framework provides the basic operational environment for a GenSAA expert system. The components of the GenSAA Runtime Framework are used without change in each GenSAA expert system. They control the operation of a GenSAA expert system during its execution.

This program was written by Peter M. Hughes of **Goddard Space Flight Center** *and Edward C. Luczak of Computer Sciences Corporation. Further information is contained in a TSP [see page 1].*

This invention is owned by NASA, and a patent application has been filed. Inquiries concerning nonexclusive or exclusive license for its commercial development should be addressed to the Patent Counsel, Goddard Space Flight Center [see page 20]. Refer to GSC-13672.

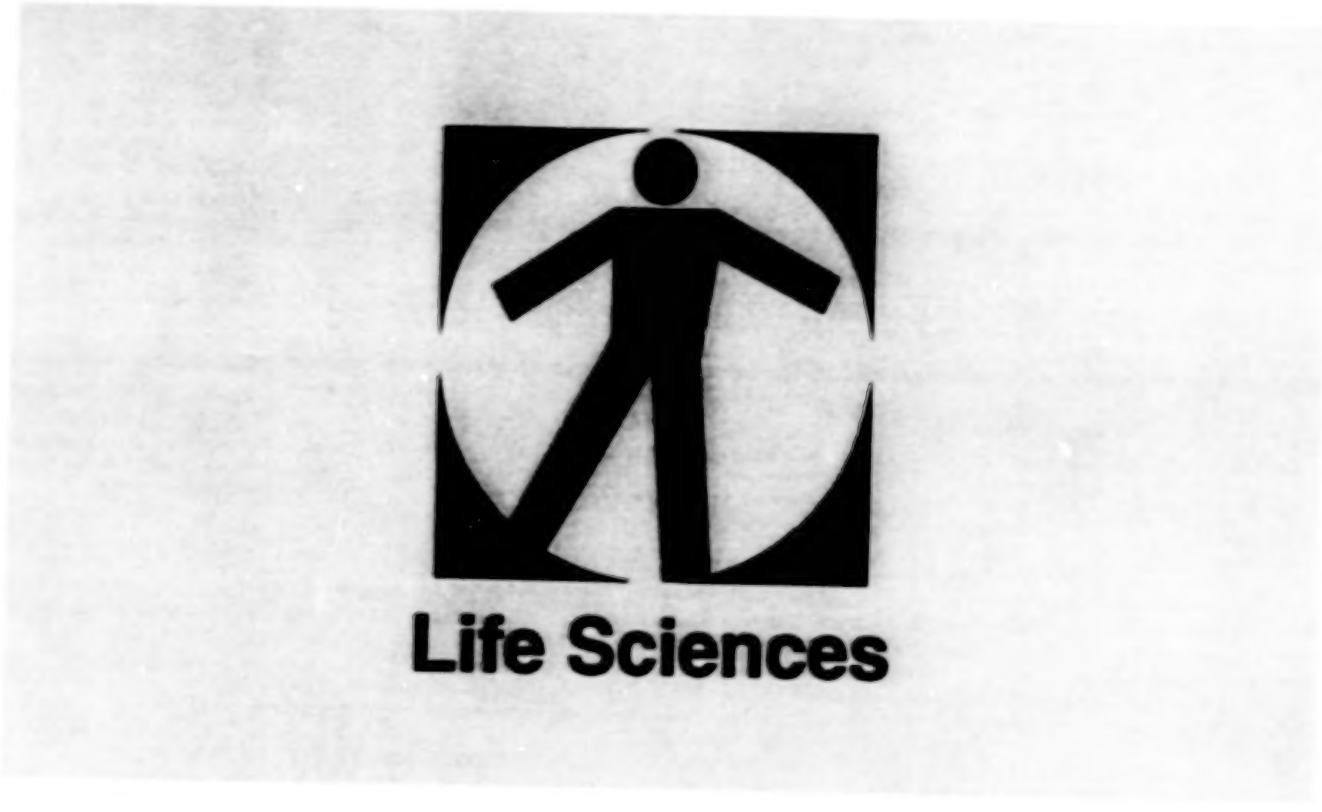

Hardware, Techniques, and Processes

55 Whole-Blood-Staining Device

Whole-Blood-Staining Device

This inexpensive, hand-held device is robust and self-contained.

Lyndon B. Johnson Space Center, Houston, Texas

A whole-blood-staining device provides a means of (1) staining white blood cells by use of monoclonal antibodies conjugated to various fluorochromes, followed by (2) lysing and fixing of the cells by use of a commercial reagent that has been diluted according to NASA safety standards. More stable than whole blood, the lysed/fixed cells can be refrigerated at a temperature of 4 °C for as long as 72 h before processing and analysis on a flow cytometer.

This whole-blood-staining device is inexpensive and easy to manufacture. It offers advantages of compactness, robustness, and simplicity in comparison with equipment developed previously for the same purpose. The device is hand-held and self-contained. The use of the device does not require electric power, precise mixing, or precise incubation times.

The device (see figure) includes a reagent tube and two clips that separate the reagent tube into three compartments. During manufacture, the three compartments are loaded with (1) a solution containing the staining antibodies, (2) a lysing/fixing solution, and (3) a buffered saline solution, respectively. The first section, which contains the antibody solution, is equipped with a septum through which the blood sample can be injected.

At the time and place of sampling, 100 µL of anticoagulated whole blood is injected into the antibody solution via the septum. The device is shaken gently for about 10 s to mix the blood cells with the staining antibodies. The device is then held at room temperature for 30 min to incubate the blood-cell/antibody mixture. Next, the clip that separates the blood-cell/antibody mixture from the lysing/fixing solution is removed, the device is again shaken for about 10 s to mix the contents, and the device is again held at room temperature for 30 min. Then the other clip is removed and the device is shaken for about 10 s to mix in the saline solution. At this point, the device is refrigerated to preserve the mixture until further processing.

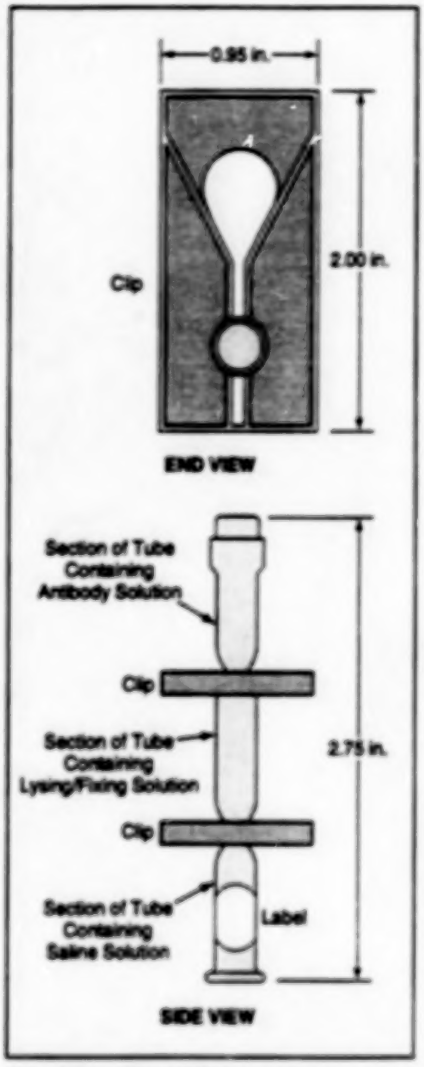

This **Whole-Blood-Staining Device** is inexpensive, simple, and easy to use.

The device was developed for use in ascertaining changes in the immune systems of astronauts during long space flights. It is also suitable for use on Earth in small facilities that cannot afford expensive automated lysing equipment, large stocks of monoclonal-antibody reagents that could expire before use, and flow cytometers. Reference laboratories could send the devices to small rural facilities or doctors' offices for staining and lysing of blood samples, and the devices could be returned with the samples for analysis.

This work was done by Clarence F. Sams of **Johnson Space Center;** *Vaughan Clift and Kelly E. McDonald of Martin Marietta Services, Inc.; and Ellen Meinelt of Krug Life Sciences. Further information is contained in a TSP [see page 1].*

This invention is owned by NASA, and a patent application has been filed. Inquiries concerning nonexclusive or exclusive license for its commercial development should be addressed to the Patent Counsel, Johnson Space Center, (281) 483-0837. Refer to MSC-22614.

END

02-18-00